Study to support the definition of Arctic Weather Satellite (AWS) high frequency channels

Patrick Eriksson, Inderpreet Kaur and Simon Pfreundschuh
Department of Space, Earth and Environment
Chalmers University of Technology
SE-412 96, Gothenburg, Sweden

Summary

The main objective of this study is to demonstrate that channels around 325 GHz can provide a basis for cloud filtering/correction of data measured around 183 GHz. Previously, it was suggested that a channel at 229 GHz to be used for cloud filtering. The 229 GHz channel forms a part of the MicroWave Sounder (MWS) and will be used for cloud filtering of 183 GHz inside that mission. In this study, we investigate the possibility to use some 325 GHz channels instead.

On basis of the relative humidity (RH) weighting functions of 183 GHz, three specifications for 325 GHz channels were suggested. A channel specific simple regression was tested to estimate and correct the impact of hydrometeors in 183 GHz channel. The advantage of this approach is that for each 183 GHz the cloud adjustment can be quantified simply through a polynomial fit between the the cloud impact in 183 GHz channel of concern and brightness temperature differences between 183 GHz and 325 GHz. A similar regression scheme based on 229 GHz was also examined, but gave poor results. One drawback of the simple correction scheme is it's channel specific approach, which cannot benefit from the other 325 GHz channels available. In order to effectively use information from all 325 GHz channels, we suggested a machine learning based approach for cloud correction. We used QRNN (Quantile Regression Neural Network) to correct the cloud impact in each 183 GHz channel using measurements from all available channels of 325 GHz. All three options of 325 GHz were evaluated, and the performance was comparable. For some channels, interestingly, the spread of errors was narrower than the noise of the target 183 GHz channel. Another advantage of using QRNN is that the cloud free values are predicted at different quantile levels, which helps in quantifying the case-specific uncertainty estimate. A similar QRNN model with 229 GHz gave poor results. No critical dependency to the 325 GHz receiver noise temperature was observed.

This study shows that combining measurements from 325 GHz can provide a better cloud correction performance than 229 GHz, and also with minimal rejection of data. The clear-sky predictions have error distributions which are symmetric with low bias and spread. Therefore, the NWP and standalone 1DVAR models that utilise the "clear-sky" data can greatly benefit from it. Also, in data assimilation systems, the case-specific uncertainty allows an effective selection of weights, thus significantly improving the impact of measurements. Another advantage of combining 183 GHz and 325 GHz for cloud correction is that NWP systems, which are not yet prepared for 325 GHz, could still benefit from the data early on.

The cloud correction analysis did not give a clear value on the relative merit of the suggested channel options and also the measurements' degree of freedom (DoF) was assessed

based on the performed simulations. The DoF can be seen as a measure of the effective number of channels. The DoF analysis gave further support for selecting 325 GHz in favour of 229 GHz. The DoF of the 325 GHz options is higher or equal to the 229 GHz one, already in clear-sky conditions, while for cloud conditions 325 GHz consistently gives two additional degrees of freedom. Some additional 325 GHz channel versions were considered in the DoF analysis.

With 325 GHz as a better option confirmed, the next step is to establish requirements for these channels. The study considered this question to some extent. The cloud correction simulations gave no clear constraints on the requirements, while the DoF analysis at least gave some indications. By comparison to the NEΔT requirements for ICI and DoF values derived, it is suggested to set threshold, target and breakthrough for the 325 GHz receiver noise temperature to 2400, 1800 and 1200 K, respectively. Regarding number, position and widths of channels, the differences between considered options are relatively small and at this point, it seems reasonable to let technical considerations guide the basic selection between having three or four channels. Later, when the technical constraints (such as the IF range available) are better known an updated assessment should be performed to set the final channel values.

Contents

1 Introduction **1**

2 Assumptions on AWS characteristics **2**

3 Input data and software **3**

4 Overview of the 183, 229 and 325 GHz bands **7**

5 Preliminary options for 325 GHz channels **10**

6 Cloud correction by a simple scheme **11**

7 Cloud correction by QRNN **21**

8 Sensitivity to different T_r **29**

9 Degrees of freedom **29**

10 Discussion **33**

11 Conclusion **38**

1 Introduction

1.1 Background

The Arctic Weather Satellite (AWS) is a small platform carrying a single radiometer package. This instrument is an across-track scanning microwave radiometer. The exact channel configuration of AWS is not yet set. The main issue for this study is that AWS will have channels at 183 GHz, but also one or several channels a higher frequencies. A number of channels around 325 GHz was considered as the main option before AWS became an ESA prototype mission, but it has now also been suggested to have a single channel at 229 GHz. This suggestion is based on MWS (MicroWave Sounder), one of the instruments onboard the next generation of Metop satellites. The 229 GHz was added to MWS as an help for performing cloud screening of 183 GHz data (Sreerekha et al. 2008). For comparison, it can be mentioned that ICI (Ice Cloud Imager), another new EPS-SG (EUMETSAT Polar System - Second Generation) sensor, will include 325 GHz channels.

1.2 Aim

To support the selection between 229 and 325 GHz channels, this report investigates the possibility to use the latter range in forming 183 GHz data of "clear-sky" character. That is, following Sreerekha et al. (2008), the assumption, is that the 183 GHz data will be used in an system not yet capable of doing "all -sky" assimilation.

In Sreerekha et al. (2008) the task was defined to screen out observations having a cloud impact exceeding 4 K at 183 ± 7 GHz. Their final suggestion for screening does not involve data from any other channel than 229 GHz, but requires radiative transfer calculations (as a "B-O test" is made). Only screening of 183 ± 7 GHz was discussed.

In this report, the task is defined in a somewhat different manner. The aim is not just to estimate the cloud impact, but also to investigate to which degree the cloud impact can be removed, i.e. to make a cloud correction. Further, in this report only schemes that can be based directly on AWS data will be considered and versions involving "B-O tests" are left for possible future studies.

1.3 Comparison to Sreerekha et al. (2008)

Results from Sreerekha et al. (2008) will be used as reference. They did not suggest specific settings of their algorithm. The main consideration of their scheme is a threshold value. We assume below 6 K for this value, as it used most frequently as example in Sreerekha et al. (2008). According to their Table 3, this results in that 2.4% of the "cloudy" cases are miss-classified as "clear". We assume that these cases have a cloud impact of 4 to 8 K (i.e. the screening is 100% successful for cloud impact above 8 K). For a 6 K threshold 41% of the "clear" cases are classified as "cloudy" and a removed in the screening process.

The selected threshold value is towards the high side of the ones considered by Sreerekha et al. (2008). A lower value improves the removal of "cloudy" cases, but the fraction of incorrectly removed "clear" cases increases quickly. For example, a threshold of 3 K decreases the miss-classification of "cloudy" cases to 0.6%, but increases the miss-classification for "clear" cases to 77%. If 183 ± 7 GHz is classified as cloudy, we assume that also the data from the other 183 GHz channels are rejected.

2 Assumptions on AWS characteristics

The assumption listed below are primarily taken for the Statement of Work (SoW), complemented with information provided by Anders Emrich at Omnisys (private communication, April 14 2020). The later data represent what Omnisys considers to be technically feasible inside the budget of the project.

2.1 Channel specifications

The specifications of channels around 166, 183 and 229 GHz are assumed to be fixed, with name, position and widths defined in Table 1. AWS channels 31 to 36 will be implemented as a single front-end, but are here still considered as two "bands", denoted as 166 and 183 GHz, to more easily separate the channels in the text.

For 325 GHz, it will be assumed that channels can be placed between 0.75 and 8.0 GHz in terms of intermediate frequency (IF), and that up to 4 channels inside this range can be implemented. There should be some gap between these channels, above 100 - 200 MHz, to facilitate the technical implementation. For comparison, Table 1 includes also the position of 325 GHz channels of ICI. As the ICI channels extend to 11 GHz in IF, they will not be considered for AWS but will be applied for demonstration and reference purposes.

For simplicity, the frequency variation of all channel responses is assumed to be rectangular. This selection shall not be interpreted as any opinion on the optimal shape of these responses; a significant deviation from a rectangular shape should be of no concern as long as the actual shape is well characterised.

2.2 Noise

The nominal receiver noise temperature, T_r of each band is listed in Table 2. The noise of data for individual channels is calculated as

$$\sigma^i = c\frac{T_r^i + T_a^i}{\sqrt{\Delta f^i \Delta t}} \tag{1}$$

where σ^i is the noise standard deviation of channel i, c is a scaling factor (see below), T_r^i is the receiver noise temperature of the channel, T_a^i is the antenna temperature of the

Channel name	Frequency [GHz]	Bandwidth [MHz]
AWS-21	89.000	4000
AWS-31	165.500	2800
AWS-32	176.311	2000
AWS-33	178.811	2000
AWS-34	180.311	1000
AWS-35	181.511	1000
AWS-36	182.311	500
AWS-4X	229.000	2000

Channel name	Frequency [GHz]	Bandwidth [MHz]
ICI-5	325.15±9.50	3000
ICI-6	325.15±3.50	2400
ICI-7	325.15±1.50	1600

Table 1: Fixed channel position and widths. The left table covers channels of AWS, with values taken from SoW. Channels AWS-31 to AWS-36 are at this moment mandatory for AWS, while AWS-4X is so far tentative. The right table lists the values of some channels of ICI (Eriksson et al. 2020).

Band [GHz]	89	166	183	229	325
T_r [K]	390	650	650	*1000*	1200

Table 2: Assumed receiver noise temperatures. The value for 229 GHz is selected by us, remaining values are present assumptions at Omnisys.

channel, Δf^i is the bandwidth (in terms of IF) of channel and Δt is the integration time.

The factor c is set to 1.2 to incorporate the additional noise caused by the calibration process. The bandwidth applied is the one found in columns 3 of Table 1. The integration time is set to match an effective 10 km resolution at 183 GHz. This time was estimated to 3 ms.

2.3 Various

The AWS satellite is assumed to be at an altitude of 600 km. Data were generated for sensor viewing angles (the angle from nadir) from 0° to 45°, in steps of 5°.

The polarisation response of the bands is not yet determined and for simplicity "quasi-horizontal" (defined in same way as for e.g. MWS) is throughout assumed. Antenna temperatures are obtained as:

$$T_a = T_b^V \sin^2(\theta) + T_b^H \cos^2(\theta) \tag{2}$$

where T_b^V / T_b^H is the brightness temperature at vertical/horizontal polarisation, respectively, and θ is the viewing angle (from nadir).

3 Input data and software

3.1 Atmospheric scenarios

3.1.1 Fascod

The Fascod dataset (Anderson et al. 1986) was used to represent different climate zones in overview calculations. The dataset consists of profiles of pressure, temperature and volume mixing ratio profiles of various atmospheric gases. Five climatologies were used: tropical (TRO), mid-latitude summer (MLS), mid-latitude winter (MLW), sub-arctic summer (SAS), and sub-arctic winter (SAW). No hydrometeors were included in simulations involving Fascod.

3.1.2 Bulk profile database

A database of atmospheric cases was created based on data from CloudSat (Stephens et al. 2002) and ERA-Interim (Dee et al. 2011). The core idea of the approach is to use CloudSat reflectivities to obtain as realistic vertical profiles of ice hydrometeors and rain as possible. No external CloudSat retrievals are involved. Instead the CloudSat reflectivities are mapped to properties for the passive simulations by assuming a particle size distribution and a particle habit, together denoted as the particle model. The process involves an inversion of the radar data, but as, the same particle model is used for that inversion and to map ice water content (IWC) and rain water content (RWC) to single scattering data when performing the passive radiative transfer calculations, the impact of clouds on the simulated AWS data is as realistic as possible. The thin clouds not

detected by CloudSat should not be of relevance for passive measurements frequencies 350 GHz. Background data (temperature, humidity, 10 m wind speed, ...) were taken from ERA-Interim, for the time and location of the CloudSat data. Liquid water content (LWC) was taken from ERA-Interim, as CloudSat has no sensitivity to the hydrometeor category.

This approach for generating atmospheric scenarios has been used by us since Rydberg et al. (2009), and more recently in e.g. Eriksson et al. (2020) and Barlakas and Eriksson (2020). It is also used in Ekelund et al. (2020), where the approach is described more in detail. In the cited articles, the sensor's footprint has been considered in varying degree, as "beam filling" must be considered at high impact of hydrometeors. As clear-sky and weak cloud interference are in focus in this study, and to save calculation time, instead CloudSat data were averaged over 10 km to form the atmospheric cases and standard 1D radiative transfer calculations are applied on each case (instead of applying an independent beam approximation inside a 2D or 3D atmosphere as done in cited works).

3.2 Radiative transfer simulations

3.2.1 ARTS

All radiative transfer calculations are made by the Atmospheric Radiative Transfer System (ARTS, Eriksson et al. (2011), Buehler et al. (2018)), version arts-2.3.1284. Models and input used for absorption and hydrometeor properties are described below. Ocean/water and land emissivities are taken from TESSEM (Prigent et al. 2017) and TELSEM (Aires et al. 2011), respectively.

Two calculations were performed for each atmospheric cases. One "clear-sky" where all hydrometeors contents were set to zero, and one "all-sky" where IWC and RWC derived from CloudSat reflectivities and LWC from ERA-Interim were included. Both sets of calculations were made by ARTS's interface to the RT4 solver (Evans and Stephens 1995). This "scattering solver" was used also for clear-sky, to avoid a possible bias between clear-sky and all-sky for insignificant hydrometeor contents. RT4 handles the first two elements of the Stokes vector, that were converted to brightness temperatures for H- and V-polarisation.

3.2.2 Absorption models

The absorption of nitrogen is modelled following Rosenkranz (1993). Nitrogen has a significant impact at least around 325 GHz at dry conditions. Also oxygen absorption follows Rosenkranz (1993). Oxygen is in this study mainly of concern for the 94 GHz CloudSat simulations. LWC was treated to be purely absorbing, based on Ellison (2007).

For water vapour the present settings in RTTOV are applied. That is, largely MPM89 (Liebe 1989) is followed, but some parameters for the 22 and 183 GHz transitions are replaced (Saunders et al. 2018, Turner et al. 2019). A smaller comparison to RTTOV has been made, that indicated an agreement better than 0.1 K in general. Deviations between 0.1 and 0.2 K were found for some channels at incidence angles above 40°.

3.2.3 Hydrometeor properties

As mentioned above, LWC is taken from ERA-Interim and is assumed to be totally absorbing. LWC is allowed to exist at temperatures below 0°C, i.e. super-cooled liquid cloud droplets are present in the simulations. In the mapping of CloudSat reflectivities to

RWC and IWC a total separation between liquid and ice phase is assumed. All scattering hydrometeors at temperatures above 0°C are assumed to be rain, and all below 0°C are assumed to be ice hydrometeors.

For RWC the particle size distribution of Abel and Boutle (2012) is applied. The PSD of IWC follows the basic formulation applied in DARDAR (`http://www.icare.univ-lille1.fr/projects/dardar`), using latest parameter values (i.e. α and β) as given by Cazenave et al. (2019). This PSD can be considered as a "two moment" scheme, but is here applied in a one moment manner by setting N_0^* (as a function of temperature) following Table 5 of Delanoë et al. (2014), and letting the radar reflectivity set the remaining moment.

Single scattering data are taken from Eriksson et al. (2018). For ice hydrometeors, three habits are applied: Perpendicular 3-bullet rosette, Large plate aggregate and Large column aggregate. In the last two cases, the aggregates are complemented with single crystal data to also cover smaller sizes. These data describe particles assumed to have a totally random orientation. To apply oriented particles is much more computationally costly and could not be accommodated inside the study.

3.3 Dataset formed

Using the simulation setup described in previous section, we simulated 125460 cases based on randomly selected CloudSat orbits during August 2015. The input data were restricted between 60°S to 60°N, and surface is below 500 m. Both clear-sky and all-sky scenarios were simulated, and no differentiation was made between the observations over water and land. 24 monochromatic frequencies were used so that each channel could be represented with sufficient accuracy. The simulations were generated for sensor viewing angles from 0° to 45°, but all the results described in this report are based on nadir viewing angle.

Since in this study, the cases with cloud impact are extremely important, we used "clear-sky thinning" to improve the representation of the cloudy cases in the dataset. Thinned dataset is a subset of the full dataset with 50% of the clear-sky cases removed (cloud impact < 0.2 K). The size of the thinned dataset is different for each channel.

3.4 Validation of simulations

A statistical comparison of the simulations to actual ATMS data, for channels 16-22 at nadir (zenith angle = 180°), is shown in Fig. 1. For the comparison, the daytime ATMS observations were selected as CloudSat operates only during the day part of the orbit since 2011. For the channels around 183 GHz, the ATMS characteristics are not fully simulated. The ATMS channel widths are considered, but as AWS is only covering the lower wing of the 183 GHz transition the upper side-band of ATMS is not included.

The overall agreement is good for all channels. For 183 GHz channels (Channels 18-22), the simulations and observations have a good agreement for the part of the PDFs matching clear-sky conditions (the main peak of the distribution), albeit the simulations have a more sharp peak. This could either be caused by a different geographical sampling of ATMS and CloudSat or to shortcomings in the ERA-Interim input data. The fraction of cloudy observations is lower in ATMS in comparison to simulations, for brightness temperatures below about 240 K. This is due to the fact that the antenna pattern is not considered in the simulations.

In the intermediate region, the simulations have a lower occurrence rate. The impact of hydrometeors should be somewhat higher in the upper side-band of ATMS, which is

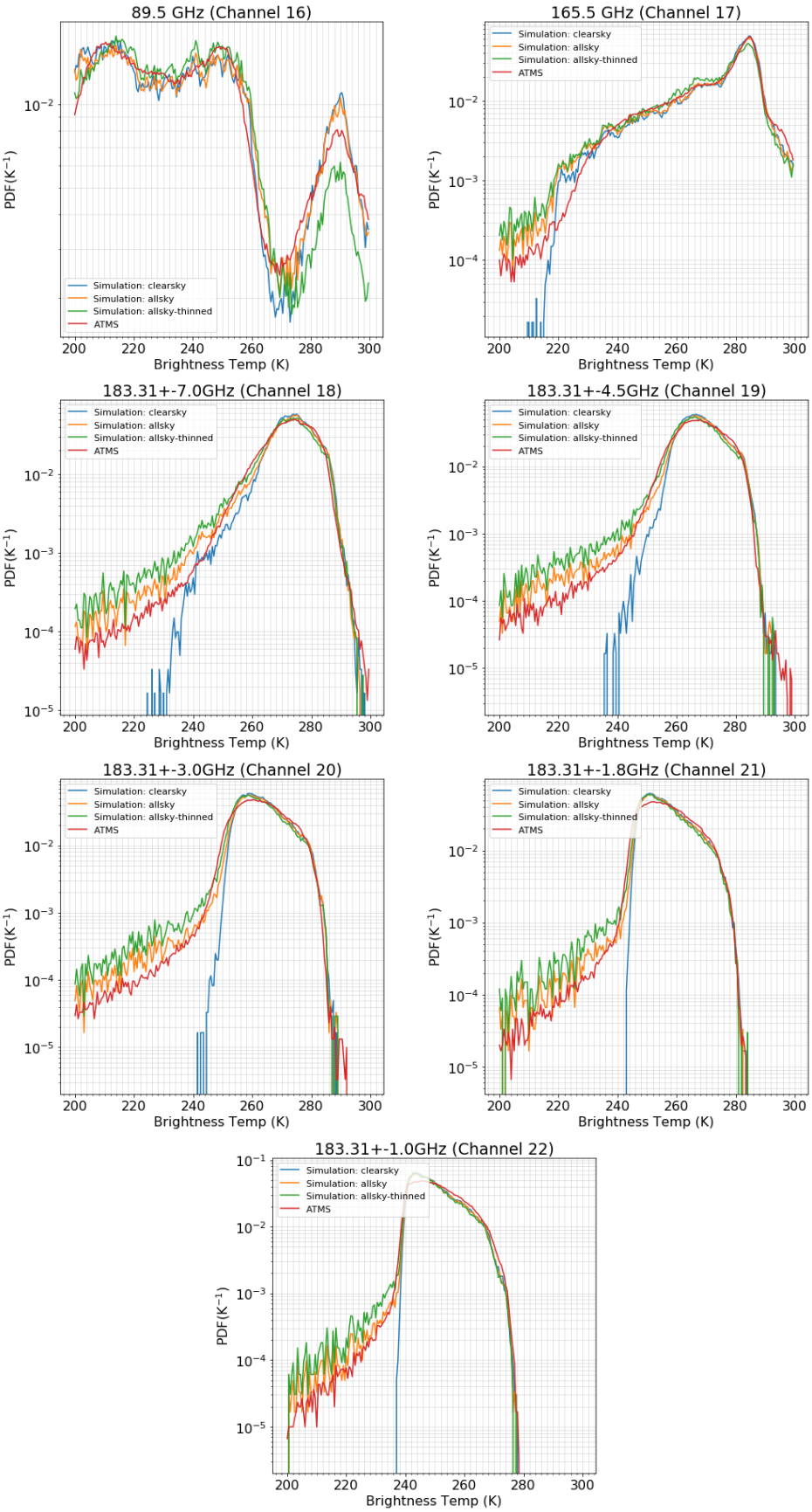

Figure 1: Probability distribution functions (PDFs) of simulated and observed ATMS channels brightness temperatures for channels 16 - 22 and nadir viewing angle. The data covers latitude range 60°S to 60°N. Both land and ocean measurements are considered and only daytime ATMS data are included. See further the text.

not reflected in the simulations, but this is not sufficient to explain the deviation. As this region is well covered in the simulations reported in Fig. 7 of Eriksson et al. (2020), the deviation of concern is presumably also a consequence of the neglected antenna pattern. In this study, this transitional region is of high interest. For this reason, the PDF for a 50% random rejection of cases with an insignificant cloud impact is also shown. This PDF gives a fair match in the intermediate region (but gives an even higher over-representation at more strong cloud impacts). This smaller dataset will be considered in parallel below, to ensure that no fraction of the "cloudy" cases is not under-represented in the results.

4 Overview of the 183, 229 and 325 GHz bands

The simulations in this section are based on five Fascod climate scenarios (Sec. 3.1.1), and performed with a fixed sensor viewing angle of 25° (deviation from nadir). No hydrometeors are included. For simpler interpretation of the results, the reflectivity is set to have no frequency variation, i.e. the same value is applied for all bands. The reflectivity is varied between 0 and 0.5 (these fixed values are only applied in this section, the bulk simulations are using TESSEM and TELSEM for setting the surface properties). In the figures covering transmissivities and Jacobians, the specifications of ICI is applied for 325 GHz channels (Table 1).

4.1 Clear-sky brightness temperatures

Figure 2 shows brightness temperatures over the three bands, for a reflectivity of 0 (i.e. a blackbody surface). The figure takes into account that the 183 GHz channels of AWS are of single-sideband character, while for 229 and 325 GHz averages of upper and lower sidebands are shown, plotted as a function from the centre frequency on the lower side.

For 183 and 325 GHz the brightness temperatures increase when moving away from the centre frequency of the transition. The "kinks" in the spectra correspond to ozone transitions, that are both more frequent and stronger in the 325 GHz range than in the 183 GHz one. See Fig. 1 of Eriksson et al. (2020) for how the ozone transitions are distributed between the lower and upper 325 GHz sideband. The spectra of 183 and 325 GHz deviate little close to the transition frequency, showing that the two frequencies are of similar strength, though the 325 GHz one is slightly weaker. The higher deviations further out in the wings are due to different contribution of far wing and continuum absorption, that is higher at 325 GHz. The 229 GHz brightness temperatures are higher than any value around 183 and 325 GHz, as expected 229 GHz being a window channel.

In Fig. 3 the surface reflectivity is changed to 0.5, which should roughly correspond to the highest reflectivity encountered at these frequencies. The differences to Fig. 2 are small for 183 and 325 GHz for the tropical and the two summer scenarios. On the other hand, there is a clear impact in the wing part of 183 GHz for the two winter scenarios. The same is true for 325 GHz, but the influence of the surface reflectivity is considerably lower. Beside for the tropical case, for 229 GHz there is a pronounced dependency of the surface reflectivity, e.g. about 35 K for mid-latitude winter.

4.2 Clear-sky transmissivities to space

Assuming that a cloud layer can be moved in altitude, its impact on measured brightness temperatures will roughly follow the transmissivity to space for the cloud altitude. In

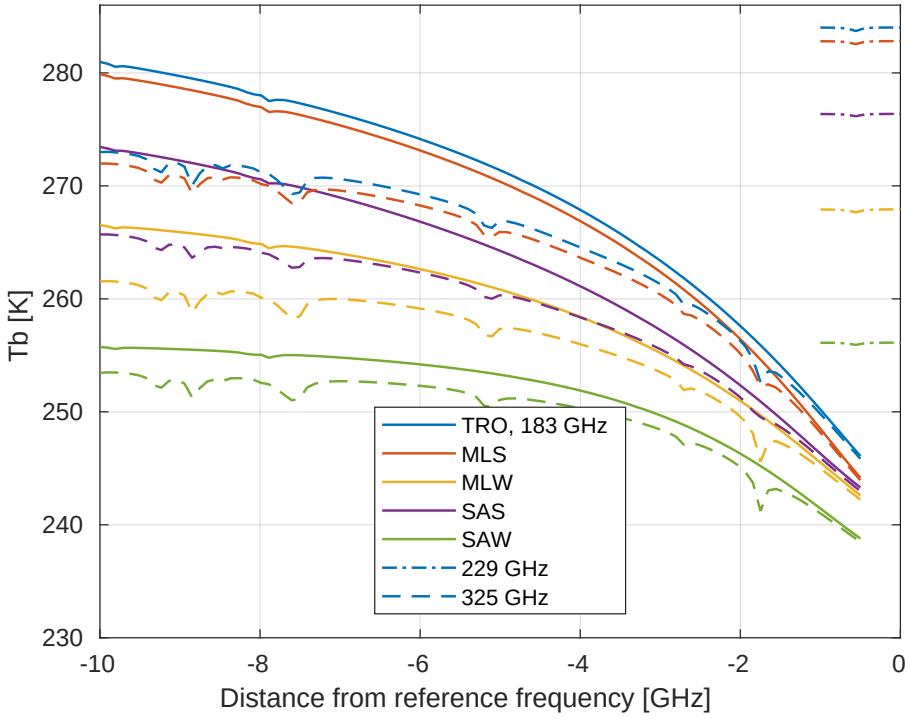

Figure 2: Solid lines show brightness temperatures for the lower wing of the 183.31 GHz transition. Dashed lines represent double-sideband measurements around 325.15 GHz, with the mean of upper and lower band shown on the low side. Dash-dotted lines represent double-sideband measurements around 229.00 GHz in the same manner, but only over the bandwidth of the potential channel. For all three bands, spectra for all five Fascod scenarios are included.

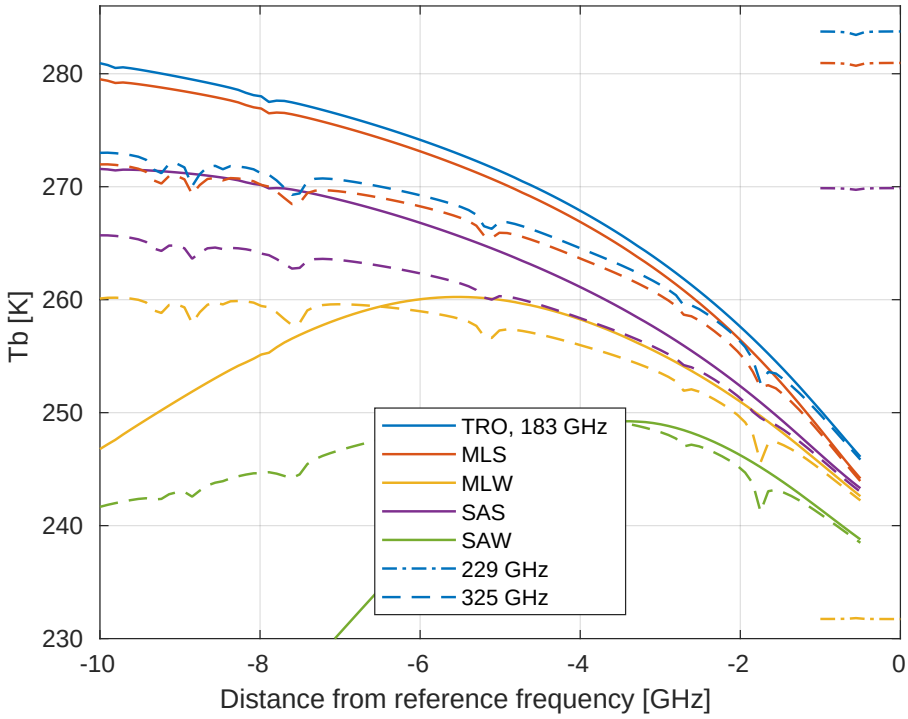

Figure 3: Same as figure above, but with a surface reflectivity of 0.5.

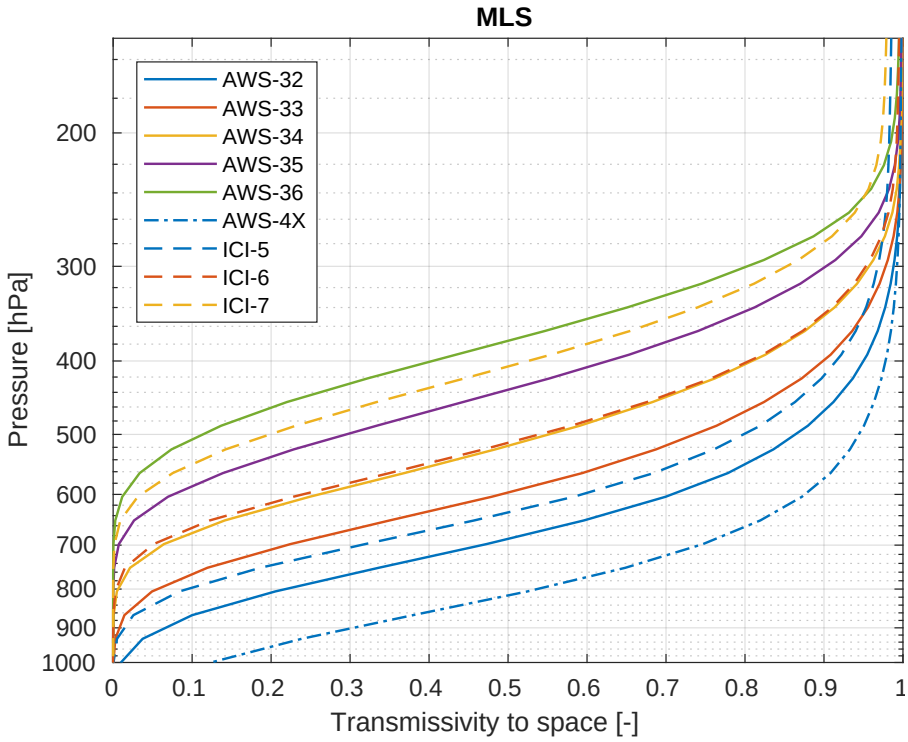

Figure 4: Transmissivity to space as a function of altitude, for the mid-latitude summer scenario. Solid lines represent 183 GHz channels, dashed lines 325 GHz channels and dashed-dotted the 229 GHz channel (Table 1). These transmissivities are independent of surface reflectivity.

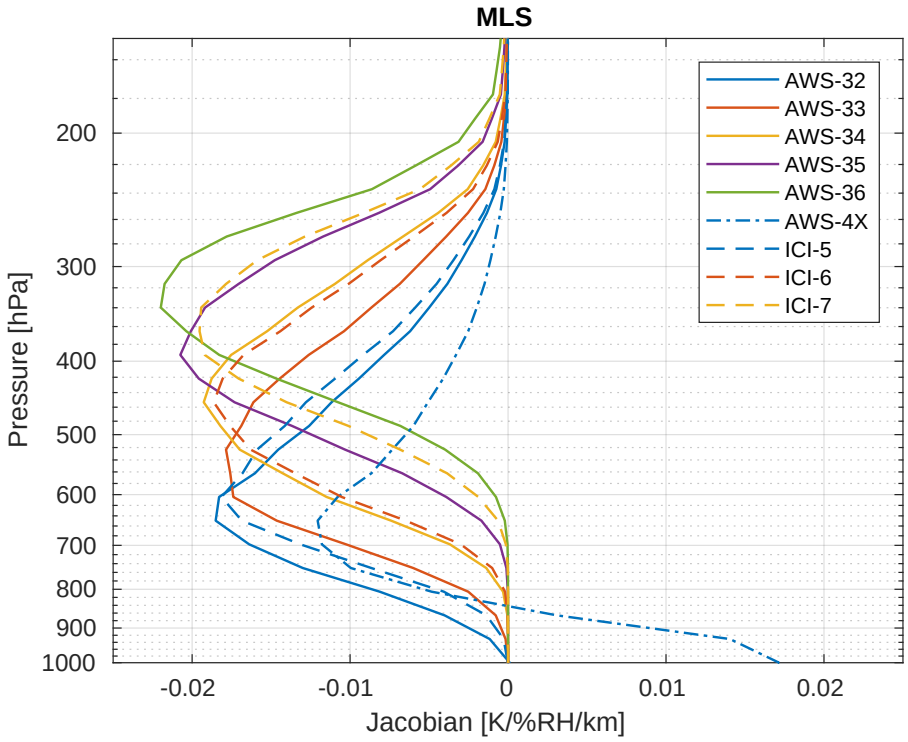

Figure 5: Jacobians for relative humidity. Line symbols as in Fig. 4. Surface reflectivity is set to 0.25.

short, where the transmissivity is zero the cloud will have no impact, while where the transmissivity is unity the influence will be close to constant with altitude (especially when the single scattering albedo is high). This relationship just refers to the relative impact for a given frequency, the absolute impact (at transmissivity 1) increases in general with frequency.

Figure 4 displays examples on transmissivities to space. The transmissivities refers to the up-welling radiation. The contribution from reflected down-welling is neglected and the considered transmissivity does not depend on surface reflectivity.

The altitude variation of transmissivity exhibits same basic shape between all the 183 and 325 GHz channels, but the altitude of optical thickness of 1 (transmissivity of $e^{-1} \approx 0.37$) varies. The curves of the edge 183 GHz channels (AWS-32 and 36) bracket the ones corresponding to the ICI 325 GHZ channels. The later channels show a higher deviation from 1 at 150 hPa, due to some (weak) ozone attenuation in the stratosphere. The 229 GHz has the highest transmissivities.

4.3 Clear-sky relative humidity weighting functions

The sensitivity to humidity is most easily compared by the channels' weighting functions (i.e. the Jacobian), and examples are found in Fig. 5. The shape of the weighting functions depends on the unity selected for representing water vapour. As the absolute amount of water vapour varies with orders of magnitude from the surface to the tropopause, it is difficult to interpret weighting functions for absolute humidity units and it is more suitable to use a relative one. In Fig. 5 the weighting functions correspond to an increase of relative humidity (RH) with one percent unit over 1 km. RH with respect liquid/ice is applied above/below 0°C.

The basic shape of the Jacobian is similar for all 183 and 325 GHz channels, but the peak altitude varies. Again the edge 183 GHz channels bracket the 325 GHz ICI ones, as for transmissivity. These Jacobians are negative, meaning that a change towards higher humidity results in decreased brightness temperatures. The 229 GHz Jacobian is positive close to the surface, as this channel has sensitivity all the way down to the surface and more water vapour just above a reflecting surface results in higher brightness temperatures. The switch from negative to positive Jacobian depends on atmospheric scenario and surface reflectivity. For dry conditions also the outer 183 and 325 GHz channels can have a positive part, as long as the reflectivity is not close to 0.

5 Preliminary options for 325 GHz channels

5.1 Impact of upper end of IF band

Figure 6 assumes that the channel placed at the high end of the IF band is 3 GHz wide (as for ICI, Table 1), and shows the RH weighting function if the outer channel ends at 11, 10, 9 or 8 GHz. The weighting functions for each sideband are here kept separated.

As expected, when the channel is moved away the centre frequency, the weighting function moves downwards. However, moving the channel from 5 - 8 GHz to 8 - 11 GHz (in IF) results only a small shift, about 400 and 200 m for the lower and upper side, respectively. In terms of the resulting double sideband channel the the shift would be 300 m. Accordingly, there is little gain by enforcing the IF range to go above 8 GHz. As a rule of thumb, a higher ratio between highest and lowest IF is more costly to implement. Albeit small, a negative consequence of a 8 - 11 GHz channel, compared to

5 - 8 GHz, is some asymmetry in the altitude response between lower and upper sideband. This asymmetry is caused by higher continuum and far wing absorption on the upper side.

In summary, the benefit of extending the IF band above 8 GHz is small and placing channels above 8 GHz seems unnecessary considering the limited budget and development time of AWS.

5.2 A three channel option

The ICI channels give a rough RH weighting functions matching with AWS-32, AWS-33 and AWS-34 (Fig. 5), and to find a tentative three channel option an even better matching was used as constrain to set the specifications. The resulting values are found in Table 3 and example weighting functions are displayed in Fig. 7. This option has a IF range of 1.0 to 8.0 GHz, and leaves a 100 MHz space between AWS-42 and AWS-43, and 200 MHz space between AWS-41 and AWS-42. That is, the suggestion uses the complete IF bandwidth as far as possible, that is technically possible. Further in the text, this channel option is denoted as "three-a".

5.3 A four channel option

The tentative four channel option in Table 4 gives a broader altitude coverage, towards higher altitudes, and offers weighting functions roughly equally spaced in altitude (Fig. 8). This option has a IF range of 0.7 to 8.0 GHz, and leaves 200 MHz space between all the 325 GHz channels. Also this suggestion uses the complete IF bandwidth. We will denote this channel option as "four".

5.4 A second three channel option

Relatively late in the study Omnisys informed us about that an IF of 1.7 GHz should be avoided, as this frequency likely will be used for downlink of data. The four channel option needed just a marginal change to adopt to this constrain, while 1.7 GHz is more or less at the centre of the three channel option. It was then decided to formulate a second three channel option, denoted as "three-b", avoiding 1.7 GHz, and the suggestion is found in Table 5.

AWS-41 is identical between the two three channel options. In this second option, AWS-43 is set to have the same limits as AWS-44 in the four channel option. AWS-42 was then allowed to fill the frequency range between the two other channels, but keeping a gap of 200 MHz on each side.

The resulting weighting functions are exemplified in Fig. 9. As expected, there is now a somewhat poorer match to 183 GHz, most importantly the weighting function of AWS-43 ends up between the ones of AWS-35 and 36. The weighting function of AWS-42 is slightly moved upwards compared to the first three channel option.

6 Cloud correction by a simple scheme

In this section, the (first) 325 GHz three channel option (three-a) is evaluated for detection and correction of cloud interference in 183 GHz channels. Combinations of brightness temperature (TB) differences between 183 GHz and 325 GHz are used as a measure of the

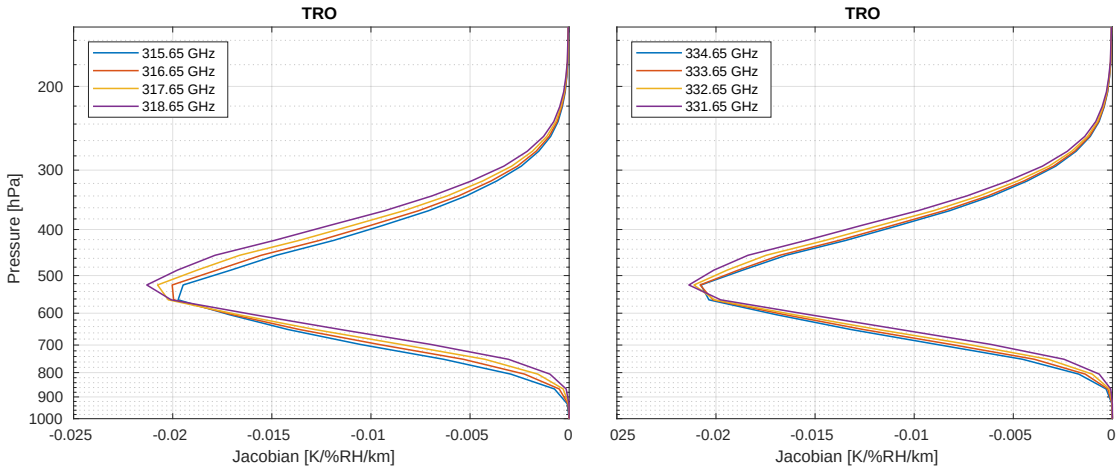

Figure 6: RH weighting functions for the lower (left) and upper (right) side of the 325.15 GHz transition. All weighting functions are for a 3 GHz bandwidth. The stated frequencies are the centre frequency of each. In terms of IF range, the channels cover 8-11, 7-10, 6-9 and 5-8 GHz (from top-to-bottom in the order given in the legends).

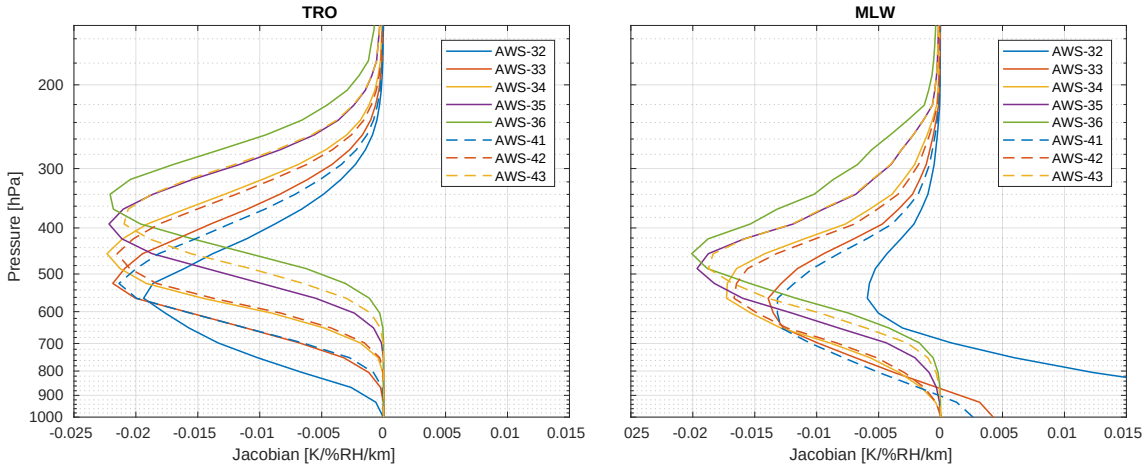

Figure 7: RH weighting functions of the three channel option in Table 3, for the Fascod tropical (left) and mid-latitude winter (right) scenarios.

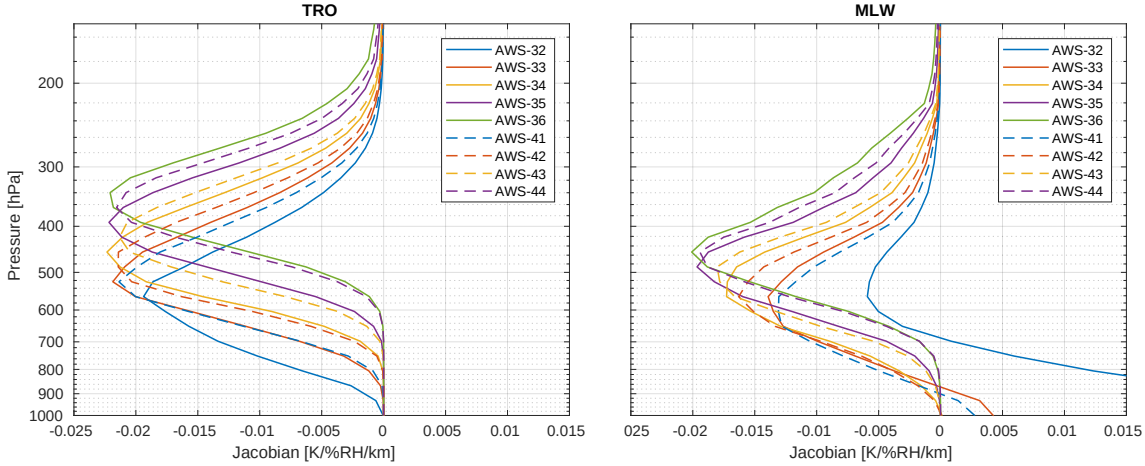

Figure 8: RH weighting functions of the four channel option in Table 4, for the Fascod tropical (left) and mid-latitude winter (right) scenarios.

Channel name	Frequency [GHz]	Bandwidth [MHz]	$T_r = 1200$ K [K]	$T_r = 1800$ K [K]	$T_r = 2400$ K [K]
AWS-41	325.15±6.50	3000	0.58	0.82	1.06
AWS-42	325.15±3.55	2500	0.64	0.90	1.16
AWS-43	325.15±1.60	1200	0.92	1.30	1.68

Table 3: Tentative suggestion for a three 325 GHz channels option (three-a). The values in the three last columns is the 1σ noise level according to Eq. 1, for $T_a = 300$ K and stated T_r

Channel name	Frequency [GHz]	Bandwidth [MHz]	$T_r = 1200$ K [K]	$T_r = 1800$ K [K]	$T_r = 2400$ K [K]
AWS-41	325.15±6.60	2800	0.60	0.85	1.10
AWS-42	325.15±4.10	1800	0.75	1.06	1.37
AWS-43	325.15±2.40	1200	0.92	1.30	1.68
AWS-44	325.15±1.20	800	1.12	1.59	2.06

Table 4: Tentative suggestion for a four 325 GHz channels option. Else as Table 4.

Channel name	Frequency [GHz]	Bandwidth [MHz]	$T_r = 1200$ K [K]	$T_r = 1800$ K [K]	$T_r = 2400$ K [K]
AWS-41	325.15±6.50	3000	0.58	0.82	1.06
AWS-42	325.15±3.30	3000	0.58	0.82	1.06
AWS-43	325.15±1.20	800	1.12	1.59	2.06

Table 5: The second three channel suggestion (three-b).

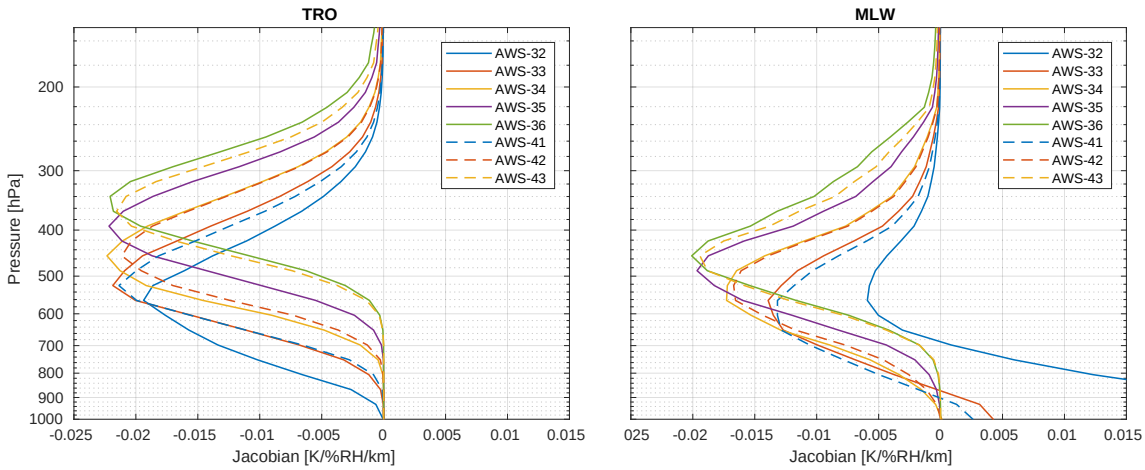

Figure 9: RH weighting functions of the second three channel option (Table 5), for the Fascod tropical (left) and mid-latitude winter (right) scenarios.

cloud impact. A regression based approach is used to estimate the adjustment needed to predict the clear-sky values.

6.1 Formulation of correction scheme

Let C1 and C2 represent one of the channels each from 183 GHz and 325 GHz, respectively, and Tb1 and Tb2 represent the corresponding TB. The correction scheme formulates a relationship between the cloud impact in C1 to the TB differences between C1 and C2:

$$Tb1_{as} - Tb1_{cs} = f(x_m) \tag{3}$$

where, $x_m = Tb2_{as} - Tb1_{as}$, and the subscripts "as" and "cs" denote the all-sky and clear-sky cases respectively.

The combinations of C1 and C2 are selected by finding best match between weighting functions. Five 183 GHz and 325 GHz combinations are possible, for example one such paired combination is AWS-34 and AWS-42.

As an example, the relationship between the TB differences for C1 and C2 and the cloud impact in C1 is shown in Fig. 10. For this particular case, C1 is AWS-34 and C2 is AWS-42, and around 125 000 simulations are used. The two variables have a reasonably strong correlation for small TB differences, but as the impact of cloud increases, the correlations gets poorer. The data can be fitted by linear or non-linear models. The fitted model can be used to obtain the adjustment required to compensate the brightness temperature for cloudy cases. To avoid fitting the "too cloudy" cases which do not show any reasonable correlation, cases with $Tb2 - Tb1 < -40$ K are excluded in the fit. Also, cases with a cloud impact below 0.2 K (red colour dots) can be considered as clear-sky, are not included in the model.

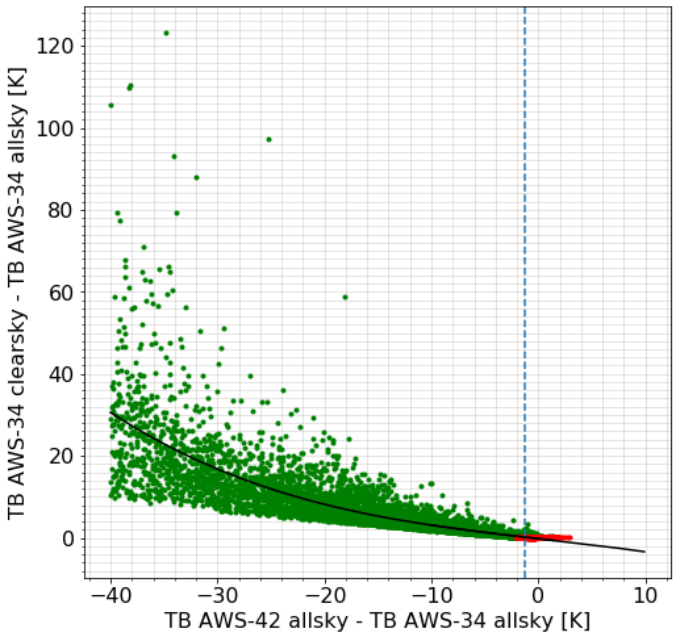

Figure 10: Brightness temperature difference of AWS-34 from AWS-42 plotted against cloud impact in AWS-34. Red and green colour represent the clear and cloudy cases respectively in the simulation dataset. The black curve represents the line of best fit (of green points) as a third order polynomial. The blue vertical line represents the correction threshold, x_{cs}, for $dtb_{cs} = 0.2$ K.

It is also important to have a manner for making a clear/cloudy classification that can be derived from actual measurement data. This is useful for making filtering in line with Sreerekha et al. (2008), but is also needed in the correction scheme. The latter is the case as the polynomial fit derived gives a non-zero correction for clear-sky cases. In Fig. 10 the difference between clear-sky values of channel C1 and C2 (red dots) have a mean close to zero (as the weighting functions are well matched), but this is not the case for all channel combinations and some general rule for finding a threshold value (with respect to x_m) must be formulated. The polynomial fit will be used also for this part.

We will simply treat cases that matches a correction below a certain value as "clear-sky". If the correction limit is denoted as dtb_{cs}, the threshold value, x_{cs}, is obtained by inverting the polynomial fit:

$$x_{cs} = f_{cs}^{-1}(dtb_{cs}). \tag{4}$$

That is, if $x_m > x_{cs}$ a measurement is classified as clear-sky. If $x_m \leq x_{cs}$, the measurement is rejected if a pure filtering is made, or it is adjusted if the correction scheme is applied. We will largely set dtb_{cs} based on the noise level of the 183 GHz channel involved, to be 1σ or 2σ where σ refers to the magnitude of measurement noise (Eq. 1, often called NEΔT (Noise Equivalent Delta Temperature)). We will use 1σ for the development of the scheme, however, the sensitivity of the scheme to a 1σ or 2σ threshold is also provided later in the text.

6.2 Application of correction scheme

In this section, we test the applicability of the correction scheme in detail. To analyse the performance of the approach, we apply it to correct the measurements from C1 using data from C2. Without the availability of actual data, the simulation dataset but with noise added is used mimic the measurements. The noise for individual channels is calculated according to Equation 1. As an example, the results from the channel combination AWS-34 and AWS-42 are shown. The error in the predicted measurements is assessed as the deviation to corresponding noise-free clear-sky value. The average bias, standard deviation and the skewness of the deviations are calculated. Skewness gives a measure of asymmetry of the probability distribution of deviations around its mean.

To test the efficacy of the correction scheme, three different models: linear, quadratic and cubic are evaluated to fit the TB differences between C1 and C2. For all three models, cases with $Tb2 - Tb1 <$ -15 K are assumed to be "too cloudy" and are not corrected. Also, cases classified as clear according to the 1σ threshold are not corrected. The clear-sky adjustment for all eligible measurements is calculated from all three models, and the three predicted datasets are compared.

The occurrence frequency of the deviations from three models is shown in Fig. 11 and their corresponding statistics are shown in Table 6. The occurrence frequency of the measurements without any filtering or correction is also plotted as reference (orange colour). If all measurements are devoid of cloud impact, the deviations should follow the Gaussian distribution of noise. In such a case, the skewness of the deviations is close to zero. However, in real conditions, the distribution has a large negative skewness due to the impact of clouds. After correction, all the three models are successful in reducing the cloud impact in the measurements. The linear model has the lowest reduction in bias (from -0.75 K to -0.03 K) but the highest values for skewness and standard deviation, in comparison to the other two models. With the linear model, the error distribution of the corrected dataset has a relatively high positive skewness, which is undesirable. The positive skewness can be due to over-correction of cloudy cases, or erroneous correction

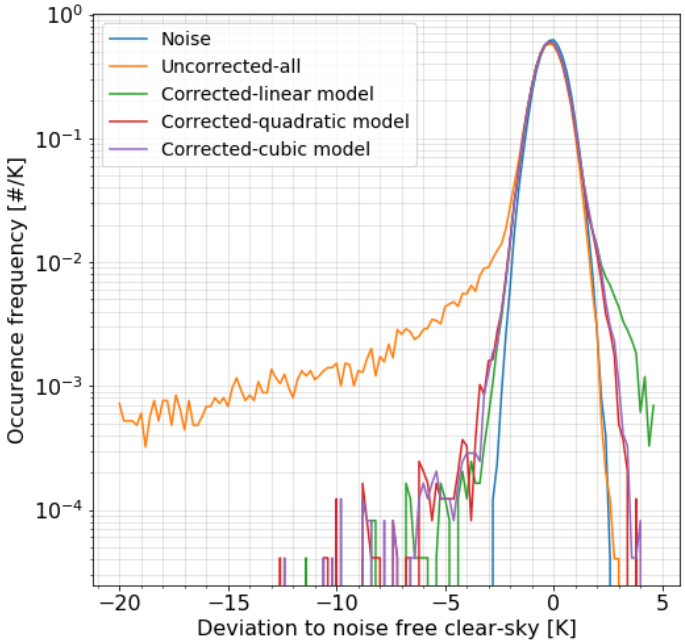

Figure 11: Deviation of AWS-34 measurements to noise free clear-sky simulations before and after correction, corrected using a linear, quadratic and cubic model. The distribution of noise alone is also shown as reference. The measurements have been corrected using brightness temperatures from AWS-42. The clear/cloudy classification is made with $dtb_{cs} = 1\sigma$ and also cases with $Tb2 - Tb1 > -15\,\mathrm{K}$ are rejected.

of clear cases. The cubic and quadratic models have almost similar statistics for bias and standard deviation, but the skewness in the cubic model is lower. Overall, the cubic model can be said to have the best performance, thus for all the results shown further, a cubic model is used.

In Sec. 3.4 the validation of simulations against ATMS data (Fig.1) showed that the cloudy cases in the simulations were underrepresented in comparison to the observations. In order to have a higher representation of cloudy cases, we thinned the measurement dataset by removing 50% of the clear-sky cases. The distribution of thinned dataset is more closer to real conditions in the region matching weak cloud impacts and all the analyses presented further in this section are based on the thinned dataset.

Figure 12 shows the deviation of the uncorrected and corrected measurements to their noise-free clear-sky values for the thinned dataset. The results from Sreerekha et al. (2008) are also shown as reference (see Sec. 1.3 for our assumptions). In order to allow a more direct comparison of our approach with Sreerekha et al. (2008), we also include the dataset, "Filtered", where all cloudy cases are rejected. Apart from the fit based cloudy classification, it is also assumed that cases with $Tb2 - Tb1 <$ -15 K are "too-cloudy" and are rejected. To analyse the sensitivity of our scheme to noise threshold, as discussed in the previous section, results from two different values of dtb_{cs} are shown. For both values of dtb_{cs} the corresponding clear-sky cut-off (x_{cs}) is calculated using Eq 4. Various metrics corresponding to the Figure 12 are shown in Table 7.

The distributions of filtered data are non-Gaussian. The right side of the distribution follows measurement noise while the left side is skewed. The skewness in the distribution

Dataset	bias [K]	std [K]	skewness [-]	fraction rejected [%]
noise	0.00	0.63	0.00	-
uncorrected-all	-0.75	4.62	-11.78	-
corrected-linear model	-0.03	0.75	0.48	2.84
corrected-quadratic model	-0.06	0.71	-0.34	2.84
corrected-cubic model	-0.05	0.72	-0.23	2.84

Table 6: Bias, standard deviation (std), and measure of skewness of error distributions shown in Figure 11. The fraction rejected describes the percentage of cases which are removed. Results from three different fit models are shown: linear, quadratic and cubic.

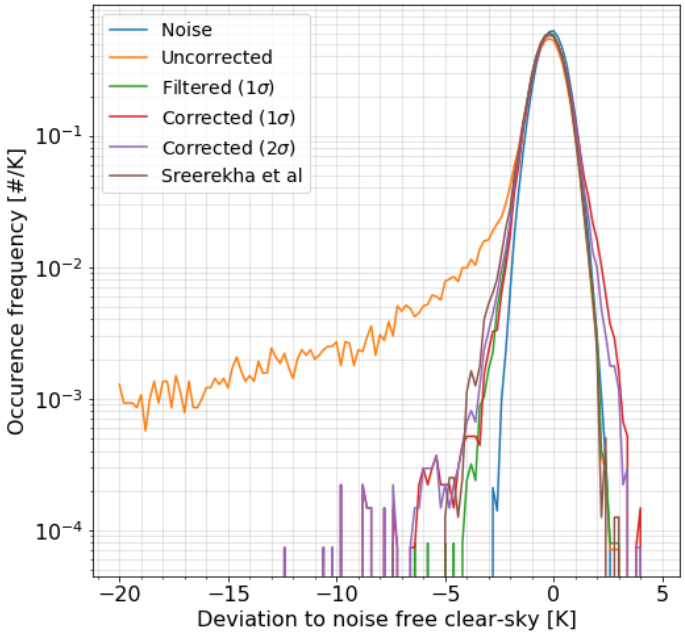

Figure 12: Deviation of AWS-34 measurements to noise free clear-sky simulations before and after correction. The measurements have been corrected using a cubic model. The different datasets are: noise (simulation dataset), uncorrected (thinned measurements), filtered 1σ (cases classified as cloudy according to $dtb_{cs} = 1\sigma$ are rejected), corrected 1σ (cases classified as cloudy according to $dtb_{cs} = 1\sigma$ are corrected), corrected 2σ (cases classified as cloudy according to $dtb_{cs} = 2\sigma$ are corrected), Sreerekha et al (cloudy cases are filtered according to Sreerekha et al. (2008)).

is due to cloud impacts which pass through the clear-sky threshold. The skewness in "Sreerekha et al" is higher than our approach because their method only aims at removing cloud impacts above 4 K. Their approach also leads to a high rejection fraction (46.37%). The filtering method introduced here, rejects only 17.54% of the data.

If the correction part for 1σ is added, the rejection is decreased even further (4.99%) and the bias is also improved (from -1.27 to -0.06 K). On the other hand, the correction gives some increase in standard deviation and skewness, compared to filtering alone. A correction using 2σ gives poorer performance, in particular the reduction in bias is smaller

and the skewness is increased.

6.3 Application of correction scheme using AWS-4X

As a reference with respect to having a channel at 229 GHz, we also apply the correction scheme described above to correct AWS-32 using AWS-4X (following Sreerekha et al. (2008)). In this case, C1 and C2 are AWS-32 and AWS-4X. The TB correlations between AWS-32 and AWS-4X are poor and show a large spread particularly for large cloud impacts (not shown). We fit the data to a polynomial model as described in Sec. 6.1 but exclude cases with $Tb2 - Tb1 <$ -20 K in the fit.

Fig. 13 shows the deviations of the measurements to clear-sky values before and after correction, and the corresponding metrics are provided in Table 8. With clear/cloudy classification for $dtb_{cs} = 1\sigma$, around 85% of the total measurements are classified as cloudy and are rejected in pure-filtering. Rejecting all the cloudy cases reduces the average bias in the measurements from -2.25 K to -0.21 K, while with the approach from Sreerekha et al. (2008) only 46.37% of the data is rejected and the average bias reduces to -0.32 K. When all the cloudy cases, except the "too cloudy", are corrected, the total bias increases to 0.88 K. The unusually high fraction of cloudy cases and an increase in bias on correction suggests misclassification of clear cases as cloudy. Since, the weighting functions of AWS-32 and AWS-4X are poorly matched, their relationship is inadequate to estimate the cloud impact in AWS-32. Without any additional information, the regression approach can only provide a successful filtering in comparison to the original approach described by Sreerekha et al. (2008), although at the cost of high rejection fraction. Additional information seems necessary to improve the accuracy of the correction.

6.4 Application of correction scheme to AWS-32, AWS-33, AWS-35 and AWS-36

The correction scheme can also be extended to other combinations of 183GHz and 325GHz channels. The most relevant combinations for clear-sky screening are: AWS-32 and AWS-41; AWS-33 and AWS-41; AWS-35 and AWS-43; AWS-36 and AWS-43.

Table 9 shows the statistics when AWS-32 is corrected using AWS-41. The bias and standard deviation of the filtered dataset are better than the approach by Sreerekha et al. (2008). However, the results from "sreerekha et al" have lower skewness. After correction, the corrected data have poorer statistics. This is not surprising as the weighting function match between AWS-32 and AWS-41 is poor. The correction using 2σ as threshold works better 1σ. This is an exception, the reverse is valid for AWS-34/42 (as mentioned) and the channel combinations discussed below.

Table 10 shows the statistics when AWS-33 is corrected using AWS-41. The TB differences for this combination and the cloud impact in AWS-33 are highly correlated. Rejecting the cloudy cases reduces the average bias in the measurements from -1.74 K to -0.13 K, while a correction of cloudy cases reduces the bias further to 0.05 K. The standard deviation and skewness of the corrected dataset are higher than pure-filtering, but smaller than the approach by Sreerekha et al. Using 2σ threshold corrects a smaller fraction of cases than 1σ but the overall statistics are poorer in comparison to 1σ, but still better than Sreerekha et al.

Table 11 shows the statistics for the combination AWS-35 and AWS-43. Here the two filtered datasets have a comparable performance, while on correction, the bias is reduced, but skewness and standard deviation are increased. After correction (1σ) the bias due

Dataset	bias [K]	std [K]	skewness [-]	fraction rejected [%]
noise	0.00	0.63	-0.01	-
uncorrected	-1.27	6.05	-8.97	-
filtered(1σ)	-0.13	0.68	-0.25	17.54
corrected(1σ)	-0.06	0.76	-0.46	4.99
corrected(2σ)	-0.11	0.75	-0.69	4.99
sreerekha et al	-0.16	0.71	-0.46	46.37

Table 7: Bias, standard deviation (std), and measure of skewness of the error distributions of datasets (AWS-34) shown in Figure 12.

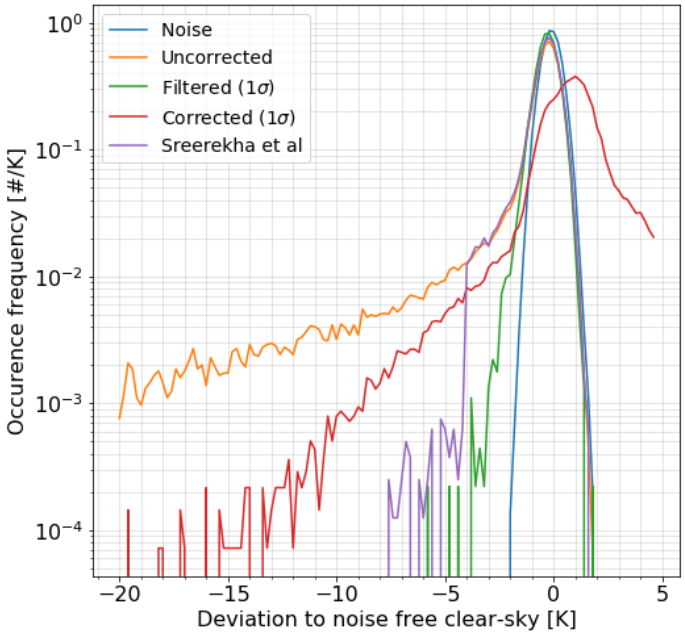

Figure 13: Same as Fig. 12, but for channel combinations AWS-32 and AWS-4X. The dataset "corrected 2σ" is not shown.

Dataset	bias [K]	std [K]	skewness [-]	fraction rejected [%]
Noise	0.00	0.45	0.01	-
uncorrected	-2.25	8.94	-6.85	-
filtered(1σ)	-0.21	0.51	-0.65	85.43
corrected(1σ)	0.88	1.76	-1.30	5.35
corrected(2σ)	0.76	1.80	-1.07	5.35
sreerekha et al	-0.32	0.78	-1.94	46.37

Table 8: Same as Table 7, but for channel combinations: AWS-32 and AWS-4X.

Dataset	bias [K]	std [K]	skewness [-]	fraction rejected [%]
noise	0.00	0.45	0.00	-
uncorrected	-2.25	8.94	-6.85	-
filtered(1σ)	-0.26	0.77	-16.33	72.06
corrected(1σ)	0.43	1.70	-14.68	7.93
corrected(2σ)	0.25	1.72	-13.86	7.93
sreerekha et al	-0.32	0.78	-1.94	46.37

Table 9: Same as Table 7, but for channel combination: AWS-32 and AWS-41.

Dataset	bias [K]	std [K]	skewness [-]	fraction rejected [%]
noise	0.00	0.45	0.00	-
uncorrected	-1.74	7.45	-7.77	-
filtered(1σ)	-0.13	0.49	-0.40	26.18
corrected(1σ)	-0.05	0.59	-0.85	6.88
corrected(2σ)	-0.11	0.57	-1.17	6.88
sreerekha et al	-0.23	0.65	-1.52	46.37

Table 10: Same as Table 7, but for channel combination: AWS-33 and AWS-41.

Dataset	bias [K]	std [K]	skewness [-]	fraction rejected [%]
Noise	0.00	0.63	0.00	-
uncorrected	-0.83	4.50	-10.85	-
filtered(1σ)	-0.13	0.68	-0.46	21.30
corrected(1σ)	0.01	0.90	-1.65	2.86
corrected(2σ)	-0.09	0.83	-2.35	2.86
sreerekha et al	-0.11	0.67	-0.22	46.37

Table 11: Same as Table 7, but for channel combination: AWS-35 and AWS-43.

Dataset	bias [K]	std [K]	skewness [-]	fraction rejected [%]
Noise	0.00	0.88	-0.01	-
uncorrected	-0.54	3.40	-12.26	-
filtered(1σ)	-0.11	0.92	-0.13	7.38
corrected(1σ)	-0.07	0.93	-0.07	2.50
corrected(2σ)	-0.11	0.94	-0.19	2.50
sreerekha et al	-0.08	0.90	-0.02	46.37

Table 12: Same as Table 7, but for channel combination: AWS-36 and AWS-43.

to cloudy measurements reduces from -0.83 K to 0.01 K while rejecting only 2.86% of the total cases. The performance of 1σ threshold in this case is also better than 2σ.

Table 12 shows the statistics when AWS-36 is corrected using AWS-43. For this combination, the weighting functions have a poor match, but the TB differences and the cloud impact are strongly correlated, as the cloud impact in AWS-36 is relatively low in comparison to other 183 GHz channels. The low fraction of rejection (7.38%) also shows that most of the measurements are without cloud impact. However, the small fraction of cloudy cases which are corrected, helps in successfully reducing the average bias from -0.54 K to -0.07 K.

7 Cloud correction by QRNN

There are two main drawbacks of the simple scheme introduced in the previous section. The filtering/correction only involves a single 325 GHz channel. The scheme could be extended to consider a higher number of channels, but there is no obvious formulation of the expressions to apply. The second problem is that no case-specific uncertainty estimate is provided, only the overall bias and standard deviations are known. The first drawback hints towards using a machine learning approach, and the second one suggests to use the special form denoted QRNN (Quantile Regression Neural Network), that was introduced for atmospheric retrievals by Pfreundschuh et al. (2018).

7.1 QRNN model

The neural network training is a process of learning to predict the outputs y_i from inputs x_i through a series of learnable transformations. While training, neural networks seek to minimise the model error through a loss function. The choice of the loss function depends on the predictive problem. When a neural network is trained to minimise the mean of the quantile loss function to predict the quantiles of the distribution, it is called a Quantile Regression Neural Network (QRNN).

If x_τ is the τth quantile of a cumulative distribution function $F(X)$, the quantile loss function is defined as:

$$\mathcal{L}_\tau(y_\tau, y_{true}) = \begin{cases} (1-\tau)|y_\tau - y_{true}| & \text{if } y_\tau < y_{\text{true}} \\ \tau|y_\tau - y_{\text{true}}| & \text{otherwise,} \end{cases} \tag{5}$$

A detailed description of QRNN can be found in Pfreundschuh et al. (2018).

7.1.1 Training

In this section, QRNNs are used to correct the cloud impact in each of 183 GHz channels using TBs measurements from all available channels of 325 GHz. A separate QRNN is used for each of the 183 GHz channels. For example, to predict clear-sky TBs from AWS-34, the training data is measurements from all channels of 325 GHz and measurements from the 183 GHz to be predicted. We assess the performance of the scheme using both three channel and four channel options of 325 GHz. Two suggestions for three channel option are described in Sec. 5, and both have been used to train QRNN separately. Thus, for each channel of 183 GHz, we have a set of three predictions: one from four channel option, and two from the options "three-a" and "three-b".

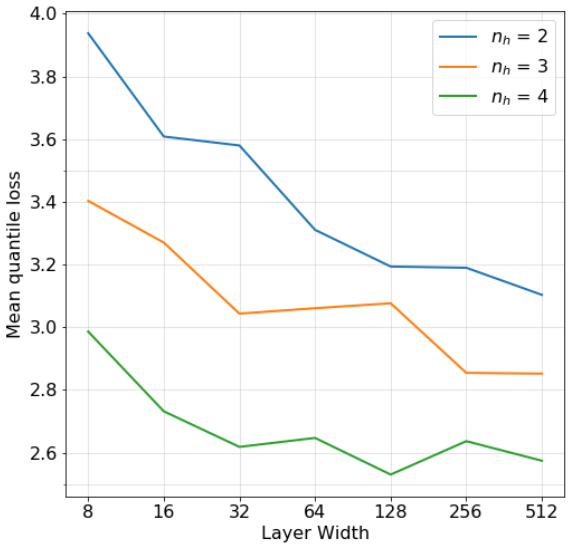

Figure 14: The mean quantile loss with different configurations of layer width and hidden layers (n_h). Here QRNN is trained to predict clear-sky values for AWS-34 using four channels option of 325 GHz

To develop the QRNN scheme, we use the same dataset as in the simple scheme . Out of 125 460 simulations, 90% are used to train the model, while the rest 10% is used to evaluate the model's performance during training. Presently we train QRNN for only nadir sensor viewing angle and the receiver noise T_r = 1200 K. In the training process, noise is added to the input according to Eq. 1, every time the training data are exposed to the model. This ensures that the model is exposed to a new dataset on every iteration. Before training, the input data is normalized with mean and standard deviation.

The structure of the QRNN is defined by various hyper-parameters which are tuned to achieve a high-performing model. These parameters determine the structure of the neural network and how the network is trained. We performed a grid search to determine structural parameters: depth (number of hidden layers) and width (number of neurons). The quantile loss on the validation set averaged over all predicted quantiles is used to compare the performance of different hyper-parameter configurations. Figure 14 shows the mean quantile loss when QRNN is trained for predicting clear-sky values for AWS-34 using four channel option. Increasing both layer width and depth has a positive impact on performance of the network, however for four hidden layers, increasing the layer width leads to only small performance gains. On basis of these results, a neural network with four hidden layers and 128 neurons was chosen. For the training, we obtained the best performance when trained with a multiple learning rate schedule. We start the training process with a initial learning rate and after a certain number of epochs, the training is updated with a new initial learning rate. We chose three training schedules with initial learning rates = 0.01, 0.001, 0.0001 respectively, updated after 20 epochs.

The grid search was also conducted for both three channel options, and an identical QRNN structure, as described for the four channel option, was found to have the best performance. For QRNN models presented here, we did not optimise the type of activation function and batch size. Rectified Linear Unit (ReLU) was used as the activation function and the batch size was set to 256 samples for all QRNN models.

7.2 Prediction accuracy

We train the QRNN to predict the quantiles x_τ, for median, $\pm1\sigma$, $\pm2\sigma$ and $\pm3\sigma$ ($\tau =$ 0.002, 0.03, 0.16, 0.5, 0.84, 0.97, 0.998). The expectation value of the posterior distribution is assumed to be the best estimate for the predicted clear-sky value. To analyse the prediction accuracy, a testing dataset was constructed by randomly drawing 25 000 cases from the simulation dataset. Noise was added to each simulation to mimic a new measurement dataset.

The distributions of the predicted clear-sky noise-free values for each of the 183 GHz channels are shown in Figure 15. The simulated clear-sky distributions are also plotted for reference. These results are from the four channel option. The distributions show that QRNN is overall successful in predicting the clear-sky cases. For all channels, the simulations and predictions have a good agreement for the main peak of the distribution. However, for AWS-32, AWS-33 and AWS-34, QRNN seems to predict slightly colder TBs. These results give an indication of the behaviour of QRNN, but for a detailed analysis of the prediction accuracy, we make a quantitative assessment of the errors.

In an analogy between the results from the simple correction scheme and QRNN, we perform a similar error distribution analysis as in Sec. 6. Figure 16 shows the error distributions of the measurements and predicted clear-sky TBs for AWS-34 using three (three-b) and four channel options of 325 GHz. Measurements with cases with $Tb2 - Tb1 > -15$ K are assumed to be too-cloudy and are filtered out. Here $Tb1$ denotes TBs from AWS-34 and and $Tb2$ is the paired counterpart from 325 GHz, i.e., AWS-42. Both the three channels and four channels QRNN models are successful in predicting the clear-sky noise-free value for AWS-34, and the resulting error distribution is symmetric. The statistics corresponding to these distributions are provided in Table 13. The fraction of cases rejected as "too-cloudy" is also provided under "fraction rejected". For AWS-34, average deviation in the predictions from all three QRNN models are comparable. The cloud impact in the uncorrected measurements is reflected in the high negative skewness (-10.32), however the predictions have relatively symmetric error distributions as reflected by the low skewness values. Among the three set of predictions, option three-b has the most symmetric error distribution but with a relatively large spread. Predictions from option four have the lowest standard deviation (0.620 K), which is interestingly smaller than the standard deviation of noise (0.641 K). Though, all three options of 325 GHz provide a full coverage to the hydrometer impact in AWS-34, predictions from four channel option have slightly better accuracy.

Similar error statistics are also estimated for other 183 GHz channels. Table 14 provides the statistics for AWS-32. Before correction, the average bias and standard deviation with respect to noise free simulations is -1.343 K and 5.908 K respectively. However, after correction (four channel), the bias and standard deviation are -0.011 K and 0.878 K. The skewness in the error distributions is also reduced in the predictions (from -7.48 to -3.03). But a relatively high negative skewness in the predicted dataset indicates presence of uncorrected cloud impact. For AWS-32, option "three-b" has the lowest spread of errors, but the error distributions are more symmetric for option "four".

Table 15 shows the statistics for AWS-33. The standard deviation in the four channel option (0.591 K) is lower than "three-b"(0.612 K), but the skewness in three-b in lower. This indicates that with four channel option, the QRNN predictions are mostly closer to the simulations, but few cases with large cloud impact are under-predicted.

For AWS-35 (Table 16), the four channels option has the best performance. The average bias in QRNN predictions (four) is only 0.04 K in comparison to -0.42 K for the

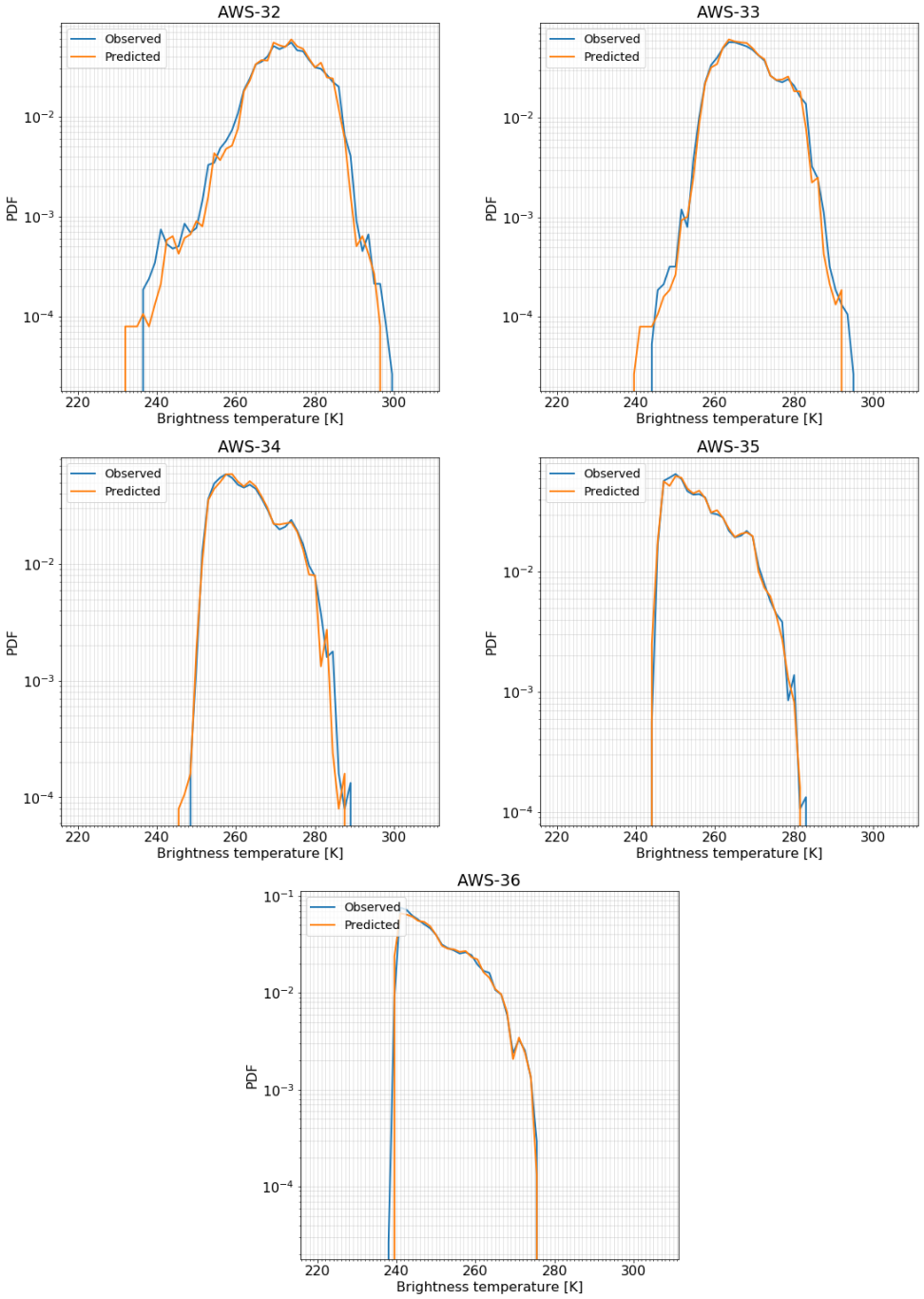

Figure 15: Probability distribution functions (PDFs) of predicted and observed noise free brightness temperatures for all 183 GHz channels of AWS. The results are based on QRNN trained with four channel option of 325 GHz.

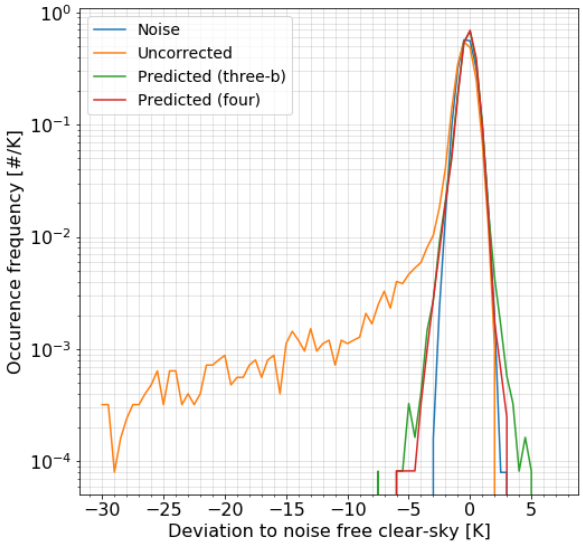

Figure 16: Deviation of AWS-34 measurements to noise free clear-sky simulations before and after correction with QRNNs. Predictions from three channel (three-b) and four channel options for 325 GHz are shown.

Dataset	bias [K]	std [K]	skewness [-]	fraction rejected [%]
Noise	0.003	0.641	-0.001	-
uncorrected	-0.677	3.673	-10.321	-
corrected (three-a)	0.094	0.624	-0.629	2.750
corrected (three-b)	0.100	0.652	-0.543	2.582
corrected (four)	0.111	0.620	-0.659	2.985

Table 13: Bias, standard deviation and measure of skewness for the error distributions of the dataset (AWS-34) shown in Figure 16. The labels "three-a", "three-b" correspond to the old and new suggestions of three channels options of 325 GHz, and the label "four" represents the four channels option.

Dataset	bias [K]	std [K]	skewness [-]	fraction rejected [%]
Noise	-0.004	0.450	-0.030	-
uncorrected	-1.343	5.908	-7.484	-
corrected (three-a)	0.019	0.889	-3.519	4.906
corrected (three-b)	-0.008	0.850	-3.326	4.926
corrected (four)	-0.011	0.878	-3.030	4.930

Table 14: Same as Table 13, but for channel AWS-32.

Dataset	bias [K]	std [K]	skewness [-]	fraction rejected [%]
Noise	-0.005	0.450	-0.004	-
uncorrected	-0.982	4.703	-8.778	-
corrected (three-a)	0.088	0.583	-0.959	4.197
corrected (three-b)	-0.030	0.612	-0.756	4.205
corrected (four)	0.106	0.591	-1.006	4.212

Table 15: Same as Table 13, but for channel AWS-33.

Dataset	bias [K]	std [K]	skewness [-]	fraction rejected [%]
Noise	0.003	0.626	-0.009	-
uncorrected	-0.428	2.653	-12.492	-
corrected (three-a)	0.060	0.610	-0.281	1.439
corrected (three-b)	0.097	0.618	0.011	1.331
corrected (four)	0.042	0.591	-0.351	1.821

Table 16: Same as Table 13, but for channel AWS-35.

Dataset	bias [K]	std [K]	skewness [-]	fraction rejected [%]
Noise	0.000	0.888	0.005	-
uncorrected	-0.269	2.059	-11.899	-
corrected (three-a)	0.062	0.797	-0.139	1.279
corrected (three-b)	0.092	0.770	-0.075	1.124
corrected (four)	0.056	0.779	-0.172	1.156

Table 17: Same as Table 13, but for channel AWS-36.

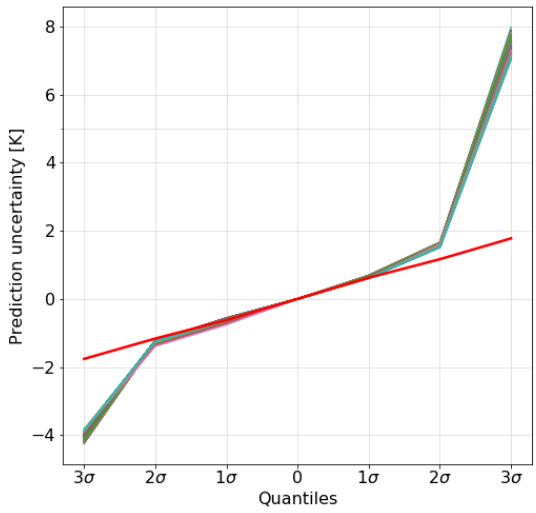

Figure 17: The prediction uncertainty in AWS-34 with respect to quantiles for randomly selected 2400 cases. The red line represents the uncertainty if underlying distribution is purely Gaussian with mean 270 K and standard deviation 0.62 K.

measurements. Option "three-b" has lower skewness than option four, but the standard deviation is higher. It is interesting to note that the standard deviation in all three predicted datasets is always lower than noise. Similar results are also seen for AWS-36 (Table 17). The four channels combination reduces the average bias from -0.269 K to 0.056 K and the standard deviation from 2.059 K to 0.779 K. Also for this channel, the spread of the predictions is narrower than noise.

7.3 Uncertainty estimation

Quantile regression can be used to construct a probability distribution of the predictions in contrast to simple regression models, which predict only a point estimate of the target. In our QRNN model, we estimate the conditional quantiles for median, $\pm 1\sigma$, $\pm 2\sigma$, and $\pm 3\sigma$. The predictions for each quantile are used to construct the confidence intervals. The confidence interval for each point estimate is a way to quantify its uncertainty. For example, the predicted quantiles for $\pm 1\sigma$ give 68% probability that the true value will lie between the range.

To inspect if the predictions follow a normal distribution, we evaluate the length of confidence intervals from the median. Figure 17 shows the prediction uncertainty in AWS-34 (four channel option). The uncertainty with respect to the median for 1000 randomly selected cases is shown. The red line represents the uncertainty in a hypothetical Gaussian distribution of 270 ± 0.62 K. If the underlying distribution is Gaussian, the prediction uncertainty should be symmetric around the median, and the uncertainties should be equally spaced for 1σ, 2σ and so on. The predictions from our QRNN model seem to be symmetric around the median for the 94% confidence interval ($\pm 2\sigma$). The figure also shows that the uncertainties for all 1000 random cases are concentrated along a narrow width, thus suggesting that the case to case variability of the uncertainty is low. A similar uncertainty quantification for other 183 GHz channels also gives similar results.

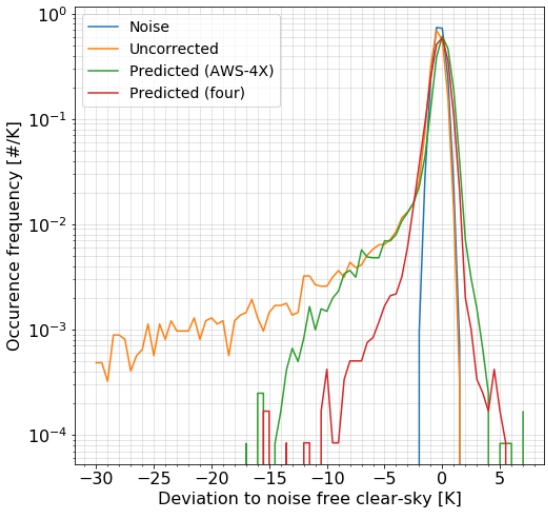

Figure 18: Error distributions for measured and predicted AWS-32, when QRNN model is trained with measurements from AWS-4X and AWS-32. The results from QRNN model trained with four channels 325 GHz are also shown for comparison.

Dataset	bias [K]	std [K]	skewness [-]	fraction rejected [%]
Noise	-0.001	0.451	0.020	-
uncorrected	-1.343	5.908	-7.484	-
corrected (AWS-4X)	0.008	1.514	-4.085	3.678
corrected (four channel)	-0.011	0.878	-3.030	4.930

Table 18: Statistics for the error distributions of AWS-32 shown in Figure 18. The QRNN model is trained with measurements from AWS-4X and AWS-32.

7.4 QRNN using AWS-4X

We also tested the QRNN model to predict cloud-free TBs by using measurements from AWS-4X and AWS-32 as input. In this case, we trained QRNN with measurements from AWS-32 and AWS-4X, to predict the clear-sky cloud free TBs for AWS-32. The model was trained as described in Sec. 7.1.1, but slightly better training results were obtained with width as 256 neurons. Other structural and training parameters remain unchanged.

Figure 18 shows the error distributions for the differences between the predicted values and clear-sky simulations for AWS-32. The corresponding statistics are shown in Table 18. The results from QRNN model trained with four channel option of 325 GHz are also shown for comparison.

When trained with AWS-4X, the predictions are not very successful in alleviating the cloud impact. Although, the error standard deviation of the predicted dataset is lower, a large negative skewness (-4.085) indicates significantly high uncorrected cloud impact. On the other hand, QRNN predictions trained with 325 GHz data are also not completely cloud free, but have a slightly better accuracy. The error standard deviation for the four channels option is 0.878 K. Clearly, without additional information, QRNN cannot learn to predict cloud free values for AWS-32. As already seen in simple correction scheme, AWS-4X is not sufficient enough to characterise the effect of hydrometeors in AWS-32.

8 Sensitivity to different T_r

In the previous section, we presented the results from QRNN trained using the three suggestions of 325 GHz proposed in Sec. 5. The receiver noise (T_r) was assumed to be 1200 K for all cases. In this section, we explore the sensitivity of QRNN to a higher receiver noise. The QRNN training is repeated for all three suggestions of 325 GHz, but with $T_r = 1800$ K and $T_r = 2400$ K. QRNN is trained with identical structural and training parameters as described earlier. Tables showing the statistics for error distributions for each channel are provided. Table 19 - Table 23 show the statistics for AWS-32, AWS-33, AWS-34, AWS-35 and AWS-36 respectively, when $T_r = 1800$ K. Similarly Table 24 - Table 28 show the statistics when $T_r = 2400$ K.

For all channels, increase in the measurement noise increases the standard deviation of the predictions. For example, for AWS-34 (four channel option), the error standard deviation is 0.620 K, 0.630 K and 0.643 K for $T_r = 1200$ K, 1800 K and 2400 K respectively. It is difficult to gauge the impact of increasing noise through bias and skewness of the error distributions, as the distribution can have a large spread, but still be symmetric with low bias and skewness. It is interesting to note that even for 1800 K, the error standard deviation for predicted values for channels AWS-34, AWS-35 and AWS-36 is smaller than noise. This is in agreement with the results seen for $T_r = 1200$ K. However, for $T_r = 2400$ K, only AWS-36 follows the trend.

Overall, the results show that an increase in the measurement noise does not have a huge impact on on QRNN accuracy. For the four channel option, with a 100% increase in noise, the change in standard deviation is less than 10%.

9 Degrees of freedom

An information content analysis is made by estimating the degrees of freedom (DoF) of the simulated measurements. The analysis is similar to the one described by Eriksson et al. (2020) for ICI.

Let $\mathbf{Y}$ be an ensemble of noise-free measurements, and $\mathbf{E}$ and $\mathbf{\Lambda}$ be the corresponding eigenvectors and eigenvalues; then in the eigenvalue space, the covariance matrix $\mathbf{S_y}$ can be written as

$$\mathbf{S_y} = \mathbf{E\Lambda E^T} \tag{6}$$

Similarly, the uncertainty due to thermal noise is

$$\mathbf{S_\Lambda} = \mathbf{E S_\epsilon E^T} \tag{7}$$

where, $\mathbf{S}_\epsilon$ is a diagonal matrix with $\mathrm{NE}\Delta\mathrm{T}^2$ as diagonal elements. The DoF is the number of diagonal elements of $\mathbf{\Lambda}$ greater than the $\mathbf{S_\Lambda}$. For further details see Eriksson et al. (2020).

To calculate the DoF, the ensemble of simulations from 89 GHz, 166 GHz, 183 GHz are used along with 229 GHz or 325 GHz. In order to compare the DoF for cloudy and clear cases, we divide the database into three parts: "all", "clear" and "cloudy'. All cases with cloud impact greater than 1 K in any of the 183 GHz channels are classified as "cloudy", otherwise they are classified as "clear". With this criteria, out of total 125460 cases, 12905 are classified as cloudy.

Dataset	bias [K]	std [K]	skewness [-]	fraction rejected [%]
Noise	-0.001	0.451	0.020	-
uncorrected	-1.342	5.908	-7.479	-
corrected (three-a)	-0.009	0.893	-3.092	4.990
corrected (three-b)	0.009	0.888	-3.197	4.902
corrected (four channel)	0.006	0.860	-2.943	4.954

Table 19: Error statistics for AWS-32, when the model is trained with $T_r = 1800\,\mathrm{K}$. The definitions of "three-a", "three-b" and "four" are same as described in Table 13

Dataset	bias [K]	std [K]	skewness [-]	fraction rejected [%]
Noise	-0.001	0.452	0.015	-
uncorrected	-0.975	4.703	-8.763	-
corrected (three-a)	0.085	0.587	-0.640	4.209
corrected (three-b)	0.062	0.605	-0.845	4.205
corrected (four channel)	0.048	0.606	-1.112	4.264

Table 20: Same as Table 19, but for AWS-33.

Dataset	bias [K]	std [K]	skewness [-]	fraction rejected [%]
Noise	0.001	0.632	0.021	-
uncorrected	-0.676	3.686	-10.301	-
corrected (three-a)	0.079	0.646	-0.344	2.730
corrected (three-b)	0.090	0.639	-0.405	2.582
corrected (four channel)	0.079	0.630	-0.399	2.981

Table 21: Same as Table 19, but for AWS-34.

Dataset	bias [K]	std [K]	skewness [-]	fraction rejected [%]
Noise	0.001	0.629	0.007	-
uncorrected	-0.417	2.654	-12.446	-
corrected (three-a)	0.045	0.636	-0.188	1.431
corrected (three-b)	0.081	0.640	-0.458	1.299
corrected (four channel)	0.058	0.617	-0.007	1.801

Table 22: Same as Table 19, but for AWS-35.

Dataset	bias [K]	std [K]	skewness [-]	fraction rejected [%]
Noise	0.002	0.882	-0.006	-
uncorrected	-0.268	2.063	-12.003	-
corrected (three-a)	0.075	0.831	-0.130	1.283
corrected (three-b)	0.105	0.807	-0.080	1.136
corrected (four channel)	0.093	0.826	-0.175	1.120

Table 23: Same as Table 19, but for AWS-36.

Dataset	bias [K]	std [K]	skewness [-]	fraction rejected [%]
Noise	0.002	0.454	0.003	-
uncorrected	-1.343	5.907	-7.483	-
corrected (three-a)	-0.017	0.877	-3.381	4.934
corrected (three-b)	-0.015	0.882	-3.177	4.974
corrected (four channel)	0.028	0.876	-3.638	4.978

Table 24: Error statistics for AWS-32, when the model is trained with $T_r = 2400\,\mathrm{K}$. The definitions of "three-a", "three-b" and "four" are same as described in Table 13

Dataset	bias [K]	std [K]	skewness [-]	fraction rejected [%]
Noise	-0.003	0.448	0.005	-
uncorrected	-0.979	4.709	-8.762	-
corrected (three-a)	0.057	0.628	-0.728	4.232
corrected (three-b)	0.040	0.614	-0.786	4.205
corrected (four channel)	0.043	0.614	-0.798	4.232

Table 25: Same as Table 24, but for AWS-33.

Dataset	bias [K]	std [K]	skewness [-]	fraction rejected [%]
Noise	-0.001	0.638	0.006	-
uncorrected	-0.676	3.688	-10.299	-
corrected (three-a)	0.069	0.655	-0.396	2.666
corrected (three-b)	0.090	0.648	-0.310	2.594
corrected (four channel)	0.059	0.643	-0.340	2.937

Table 26: Same as Table 24, but for AWS-34.

Dataset	bias [K]	std [K]	skewness [-]	fraction rejected [%]
Noise	-0.004	0.633	0.021	-
uncorrected	-0.420	2.654	-12.449	-
corrected (three-a)	0.034	0.646	-0.389	1.479
corrected (three-b)	0.076	0.647	-0.148	1.291
corrected (four channel)	0.044	0.632	-0.188	1.809

Table 27: Same as Table 24, but for AWS-35.

Dataset	bias [K]	std [K]	skewness [-]	fraction rejected [%]
Noise	0.005	0.884	-0.026	-
uncorrected	-0.268	2.057	-11.977	-
corrected (three-a)	0.039	0.854	-0.131	1.283
corrected (three-b)	0.090	0.839	-0.096	1.108
corrected (four channel)	0.059	0.850	-0.140	1.140

Table 28: Same as Table 24, but for AWS-36.

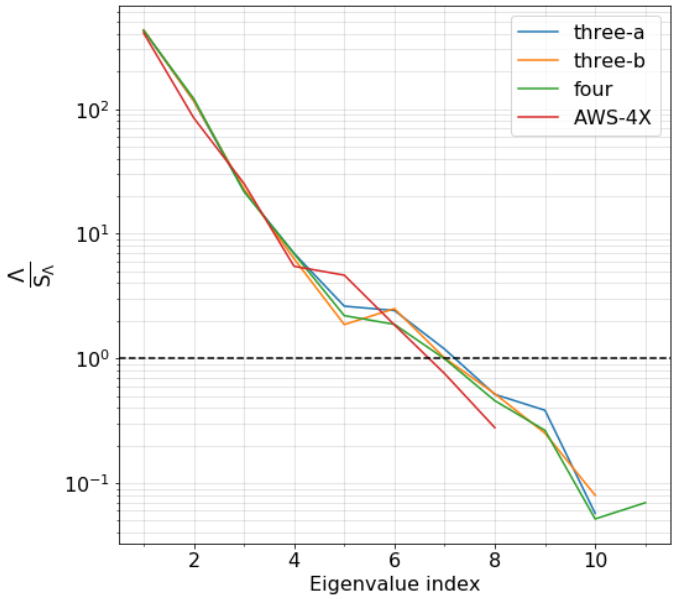

Figure 19: The ratio of Λ/S_Λ with respect to the eigenvalue index for clear-sky cases. The black dotted line represents the level where the ratio is unity.

As an example, Fig 19 shows the ratio of Λ/S_Λ with respect to the eigenvalue index for clear-sky cases. The DoF in the section below, is an interpolation between the last index having a ratio above one and next index.

9.1 DoFs for nominal IF range

At this point we got a feedback from Omnisys that also channel option three-b is technically challenging. In short, it is significantly more difficult to implement a 3 GHz wide channel at an IF of 3.3 GHz (AWS-42) than compared to at 6.5 GHz (AWS-41). To decrease the ratio between channel widths and centre IF, a third three channel option was formulated (Table 29) that is below denoted as "three-c". This option uses the same IF range as the previously suggested ones.

Table 30 shows the DoF with 325 GHz when all cases are considered. For $T_r = 1200$ K, the DoF from all four options is around 8, however, increase in receiver noise leads to a loss in the DoF. Tables 31 and 32 show the DoF for clear-sky and cloudy cases respectively. For clear-sky situations, the DoFs are about 7. With increase in T_r, the DoF are degraded. For $T_r = 2400$ K, we have only 5 DoF for option three-a and 4.8 for both option three-b/c and 4.9 for option four. On the other hand, the presence of clouds increases the DoF significantly. For all three options, we have DoF close to 9. Increase in noise has a lower effect on the DoF for cloudy cases.

The DoF values should not be interpreted to strongly. There appears to be some "noise" in the DoF, especially for higher noise. For example, in Table 30 all the options have fairly similar DoF for $T_r = 1800$ K while for $T_r = 2400$ K there are considerable differences. This shift when going $T_r = 2400$ K is not observed in the two other tables. Having this in mind, it seems that options three b and c give very similar DoF. If something, option three-c seems slightly better. The four channel option obtains somewhat lower DoF than the three channel ones.

Table 33 gives the DoF, with 229 GHz channel. The DoF is 6.8 for both clear and cloudy situations. This is consistent with the fact that 229 GHz has no redundancy

with the five 183 GHz channels, but there exists some redundancy with the two window channels (89 and 166 GHz).

9.2 Impact of extending the IF range

As a basic investigation of the impact of changing the width of the IF range, a version of the four channel option was considered, denoted as "four-b". It was modified to cover 0.7 to 9.0 GHz (instead of 0.7 to 8.0 GHz). To focus on the extension, only the edge channels were changed. That is, the revised AWS-41 and AWS-44 have bandwidth of 3.8 and 0.9 GHz, respectively. The DoFs obtained for four-b are found in Table 34.

As expected a slight improvement of the DoF can be seen for four-b. The exception "all" and $T_r = 2400$ K, again is likely an indication on some noise in the DoFs coming out of the analysis.

The results indicate that a broader IF range should give slightly better performance. If a broader IF range is feasible, the position and width of all channels should be revised, but this is out of the scope of this study, and anyhow hardly motivated before it is known more exactly to what extent the IF range can be extended.

10 Discussion

10.1 229 vs. 325 GHz

10.1.1 Altitude coverage

This discussion is based on figures and text found in Sec. 4. A basic remark is that a channel at 229 GHz channel has a lower sounding altitude than all the 183 GHz channels for clear-sky conditions. Accordingly, there are no matching RH weighting functions between 229 GHz and 183 GHz channels. On the other hand, channels around 325 GHz have quite similar characteristics as some of the 183 GHz channels (for clear-sky), but consistently have a sounding altitude above the one of AWS-32.

With respect to sensitivity to hydrometeors, 229 GHz will react on rain and clouds at lower altitudes than the 183 GHz channels. Due to the lower sounding altitude, 229 GHz is also more influenced by the surface. Both these aspects could be beneficial in a wider perspective, but are not ideal for cloud filtering of 183 GHz data. With respect to this application, the main drawback of the 325 GHz region is the lack of a full coverage for AWS-32. There exists an altitude range where hydrometeors have an impact on AWS-32 but will largely be undetected by the 325 GHz channels.

10.1.2 Performance of the basic scheme

A simple approach for cloud filtering/correction based on 325 GHz data is tested in Sec. 6. The approach requires simulations for deriving some parameters (in the form of a polynomial fit), while the application only involves measurement data. Another advantage of the approach is that it is channel specific. That is, it could result in that e.g. AWS-32 and 33 are rejected, while that data for the higher peaking channels still can be used.

The results for AWS-33, 34, 35 and 36 should be considered as satisfactorily. In short, a relatively low rejection rate is achieved and still data with relatively narrow and symmetric error distributions are provided. The lowest standard deviation and skewness are

Channel name	Frequency [GHz]	Bandwidth [MHz]	$T_r = 1200\,\mathrm{K}$ [K]	$T_r = 1800\,\mathrm{K}$ [K]	$T_r = 2400\,\mathrm{K}$ [K]
AWS-41	325.15±6.25	3500	0.54	0.76	0.98
AWS-42	325.15±3.05	2500	0.64	0.90	1.16
AWS-43	325.15±1.20	800	1.12	1.59	2.06

Table 29: The third three channel suggestion (three-c).

325 GHz option	DoF		
	$T_r = 1200\,\mathrm{K}$	$T_r = 1800\,\mathrm{K}$	$T_r = 2400\,\mathrm{K}$
three-a	8.3	7.9	7.8
three-b	8.5	8.2	6.0
three-c	8.5	8.2	7.7
four	8.2	7.8	6.2

Table 30: The degrees of freedom for AWS with 325 GHz channel. Both clear and cloudy cases are considered. Results for all three options of 325 GHz and different T_r are shown.

325 GHz option	DoF		
	$T_r = 1200\,\mathrm{K}$	$T_r = 1800\,\mathrm{K}$	$T_r = 2400\,\mathrm{K}$
three-a	7.3	7.1	5.0
three-b	7.0	6.7	4.8
three-c	7.0	6.6	4.8
four	7.0	6.0	4.9

Table 31: Same as Table 30, but only for clear cases.

325 GHz option	DoF		
	$T_r = 1200\,\mathrm{K}$	$T_r = 1800\,\mathrm{K}$	$T_r = 2400\,\mathrm{K}$
three-a	8.9	8.7	8.5
three-b	8.9	8.7	8.6
three-c	8.9	8.8	8.7
four	8.7	8.5	8.3

Table 32: Same as Table 30, but only for cloudy cases.

	DoF
all	6.8
clear	6.8
cloudy	6.8

Table 33: The degrees of freedom for AWS with 229 GHz channel.

	325 GHz option	DoF		
		$T_r = 1200\,\mathrm{K}$	$T_r = 1800\,\mathrm{K}$	$T_r = 2400\,\mathrm{K}$
all	four	8.2	7.8	6.2
	four-b	8.3	8.0	6.1
clear	four	7.0	6.0	4.9
	four-b	7.0	6.4	4.9
cloudy	four	8.7	8.5	8.3
	four-b	8.8	8.6	8.4

Table 34: The degrees of freedom for channel option four-b. Values for option four are repeated from Tables 30-31.

obtained by just performing a filtering. Activating the correction part (with 1σ as threshold value) decreases the bias and rejection rates significantly, but comes with the cost of increased standard deviation and skewness. However, the increase in standard deviation is throughout below 50% (compared to the ideal case of that the error distribution only consists of noise).

For AWS-32, filtering based either AWS-4X or AWS-41 has a very high rejection rate, though the resulting dataset has low error. The high fraction of rejection can increase the probability of removing "true" clear cases. After correction, the error distributions are asymmetric and have large bias and standard deviation. Among the two combinations, the dataset corrected with AWS-41 has slightly better bias and standard deviation. As an exception to other 183 GHz channels, the correction scheme for AWS-32 works better for 2σ threshold, as with a larger value of noise, relatively smaller number of cases are corrected. The effect of mismatch between weighting functions for AWS-32 and AWS-4X/41 is reflected in the performance of our correction scheme.

10.1.3 Comparison to Sreerekha et al. (2008)

Results from Sreerekha et al. (2008) has been used as reference, but the comparison should only be considered as being qualitative. A more detailed comparison is not possible as the selection of atmospheric cases is very different between the studies. While in this study we aim to have a statistical distribution as close as possible to real conditions, there is a strong focus on cloudy conditions in the simulations used by Sreerekha et al. (2008). Our translation of the performance reported in Sreerekha et al. (2008) to our conditions is found in Sec. 1.3.

The results of Sreerekha et al. (2008) are better than ours for AWS-32, while for the other 183 GHz channels better results are obtained by using 325 GHz data. However, when only pure-filtering is considered, our scheme performs better for AWS-32, albeit with a high rejection rate. For all later channels of 183 GHz, we reject only a small fraction of cases in comparison to Sreerekha et al. (2008), but the corrected datasets have a more symmetric error distributions with lower bias and standard deviation. Only for AWS-35 and AWS-36, the standard deviation and skewness of the corrected dataset are higher.

It should be noted that the approach of Sreerekha et al. (2008) involves simulations for every case, to obtain a "background minus observation" difference, while in this study a similar or better performance is obtained from using measurement data alone.

10.1.4 Performance of QRNN

In Sec. 7 we use QRNN as a method for cloud correction based on 325 GHz data. Measurements from all 325 GHz channels and the 183 GHz channel to be predicted are used to train the QRNN model.

The results demonstrate that QRNN is successful in predicting the clear-sky noise-free data for AWS-33, AWS-34, AWS-35 and AWS-36. The error distributions for the predictions are symmetric and have low bias and standard deviation. In fact, for AWS-34, AWS-35 and AWS-36, the spread of errors is even smaller than the noise. This is the case as a low fraction of the measurements have a significant cloud impact, and for clear sky situations the QRNN prediction can largely be seen as a weighted mean between the two channels. This averaging cancels out some of the noise in the two channels. QRNN seems to perform equally well with three configurations suggested for 325 GHz channels.

For AWS-32, the QRNN trained with 325 GHz is only partially successful in reducing the impact of hydrometeors. The resulting error distributions have significantly lower spread than the measurements, but are still negatively skewed. Among the three combinations of 325 GHz, the four channel option has slightly better performance. Since 325 GHz cannot provide a full coverage for hydrometeor impact in AWS-32, QRNN cannot learn to predict cloud free values for instances which lie outside the area of coverage. In order to compare the 229 GHz channel with 325 GHz, QRNN was also trained with AWS-4X to predict cloud free AWS-32. The performance of QRNN trained with AWS-4X is worse than training with 325 GHz. The spread of error distributions is 1.5 times more than obtained with four channels option of 325 GHz.

10.2 Technical recommendations

The cloud correction and filtering results gave no clear indications on the requirements of the channels, and as a complement, the measurements' degree of freedom (DoF) was also assessed. The latter analysis gave a bit clearer indication and the discussion in this section is mainly based on the DoF results.

10.2.1 NEΔT requirement

No critical dependency of the cloud correction to the 325 GHz receiver noise temperature (T_r) was found (Sec. 8). For example, for AWS-36 and the four channel option, the standard deviation only increased 0.85 from 0.7 when increasing T_r to 2400 K from 1200 K. The DoF showed a higher sensitivity to T_r, especially when going from 1800 K to 2400 K and only considering clear cases (Table 31).

ICI-5 has a width of 3 GHz and has NEΔT requirement of 1.2 K (Eriksson et al. 2020). From e.g. Table 5 it can be understood that this scales to a requirement on T_r of about 2700 K (as 3 GHz bandwidth and $T_r = 2400$ K gives a noise of 1.06 K).

Combining the observations drawn in the two last paragraphs it seems reasonable to set the threshold, target and breakthrough for NEΔT of AWS 325 GHz channels to match a T_r of 2400, 1800 and 1200 K, respectively. The threshold value provides a sufficient basis for an acceptable cloud correction and still represents a step forward compared to ICI. However, if the present ambition of Omnisys of $T_r = 1200$ K will be reached, AWS will provide much less noisy 325 GHz observations than ICI, representing a breakthrough.

10.2.2 Channel specifications

We formed three 325 GHz channel options. All three options were considered first in the QRNN part as it is difficult to maintain the full information of all channels in a simple regression based scheme. None of the three options gave consistently best results, and it is not possible to give a clear recommendation. For this reason we did not see any value in testing further options in this part.

Some further channel options were included on the DoF analysis. Staying inside 0.8 - 8.0 GHz in terms of IF, the option three-c was found to have the highest overall DoF, but the differences to three-b and four are relatively small. However, it could be challenging to implement any of the three channel options. The option three-a risks to be affected by interference of the downlink and in the options three-b and c there is a high ratio between bandwidth and centre IF of AWS-42. The latter aspect also makes it hard to extend options three-b and c, if it would turn out that the IF range can be extended. A brief analysis showed that a broader IF range gives some increase in DoF, that potentiallyacould improve the merit of the four channel option.

We don't see how these results can be boiled down to threshold, target and break-through requirements. Option three-c came out best here, but no full optimization of the options was made, and a modified or extended four channel version could possibly reach the same performance. In any case, the differences between the options are small, and it seems reasonable to allow that the technically most simple option is selected (that in fact can be the four channel one). When this selection is done and the technical constraints are better known (IF range available, needed frequent gaps between channels etc.), an iteration of DoF analysis should be made to see if some "optimization" of the channel specifications can be achieved.

Further, the simulations have assumed rectangular shaped response functions. This was done for simplicity and shall in no way be taken as an indication on that this shape is required. We have left some frequency gaps between the channels to simplify the technical implementation, i.e. to decrease the demand on very sharp transitions from high to low response, but if gaps of 200 MHz actually are required or if some overlap of the responses can be tolerated is not known to us.

10.2.3 Polarisation response

Polarisation aspects have not been considered in full detail. Some polarisation is induced by the surface in the simulations, but hydrometeors are assumed to be totally randomly oriented and do not cause polarisation. To involve oriented particles was not possible due to the limited time allocated for the study.

The basic recommendation would be to use the same polarisation response as far as possible. If both quasi-horizontal and quasi-vertical bands must be applied, the recommendation prioritises to use the polarisation option for 183 and 325 GHz, to maintain a similar influence of polarisation between the bands.

11 Conclusion

This study compares the options of having a channel at 229 GHz or having some around 325 GHz from a single perspective, cloud filtering/correction of 183 GHz data. There could be other important reasons to consider for the selection.

It is demonstrated that the 325 GHz channels are capable of providing a more accurate cloud correction for 183 GHz than the 229 GHz channel. The simple regression based approach evaluated is channel specific, and involves the 325 GHz channel one at a time. In the second correction approach based on machine learning, QRNN is used to predict the clear-sky noise-free values throughout using all 325 GHz in parallel. This seems to be a very useful approach. The QRNN predictions result in error distributions with low skewness and widths. In some cases, the prediction uncertainty is even lower than the noise of the 183 GHz channel targeted. This approach should be ideal for making use of AWS in assimilation systems of clear-sky type.

No results gave strong constraints for defining threshold, target and breakthrough requirements, but a suggestion is still given with respect to receiver noise temperature. The three requirements levels are suggested to be placed at 2400, 1800 and 1200 K. On the other hand, the differences found between the tested three and four channel options are too small to motivate any clear recommendation. It seems reasonable to instead select between having three or four channels based on the technical challenges associated with each option and later setting the exact channel specifications.

References

Abel, S. and Boutle, I.: 2012, An improved representation of the raindrop size distribution for single-moment microphysics schemes, *Q. J. R. Meteorol. Soc.* **138**(669), 2151–2162.

Aires, F., Prigent, C., Bernardo, F., Jiménez, C., Saunders, R. and Brunel, P.: 2011, A Tool to Estimate Land-Surface Emissivities at Microwave frequencies (TELSEM) for use in numerical weather prediction, *Q. J. R. Meteorol. Soc.* **137**(656), 690–699.

Anderson, G. P., Clough, S. A., Kneizys, F., Chetwynd, J. H. and Shettle, E. P.: 1986, AFGL atmospheric constituent profiles (0-120 km), *Technical report*, Air Force Geophysics Lab.

Barlakas, V. and Eriksson, P.: 2020, Three dimensional radiative effects in passive millimeter/sub-millimeter all-sky observations, *Remote Sensing* **12**(3).

Buehler, S. A., Mendrok, J., Eriksson, P., Perrin, A., Larsson, R. and Lemke, O.: 2018, ARTS, the Atmospheric Radiative Transfer Simulator – version 2.2, the planetary toolbox edition, *Geosci. Model Dev.* **11**(4), 1537–1556.

Cazenave, Q., Ceccaldi, M., Delanoë, J., Pelon, J., Groß, S. and Heymsfield, A.: 2019, Evolution of DARDAR-CLOUD ice cloud retrievals: New parameters and impacts on the retrieved microphysical properties, *Atmos. Meas. Tech.* **12**(5), 2819–2835.

Dee, D. P., Uppala, S. M., Simmons, A. J., Berrisford, P., Poli, P., Kobayashi, S., Andrae, U., Balmaseda, M. A., Balsamo, G., Bauer, P., Bechtold, P., Beljaars, A. C. M., van de Berg, L., Bidlot, J., Bormann, N., Delsol, C., Dragani, R., Fuentes, M., Geer, A. J., Haimberger, L., Healy, S. B., Hersbach, H., Hlm, E. V., Isaksen, L., Kllberg, P., Khler, M., Matricardi, M., McNally, A. P., Monge-Sanz, B. M., Morcrette, J.-J., Park, B.-K., Peubey, C., de Rosnay, P., Tavolato, C., Thpaut, J.-N. and Vitart, F.: 2011, The ERA-Interim reanalysis: configuration and performance of the data assimilation system, *Q. J. R. Meteorol. Soc.* **137**(656), 553–597.

Delanoë, J., Heymsfield, A. J., Protat, A., Bansemer, A. and Hogan, R.: 2014, Normalized particle size distribution for remote sensing application, *J. Geophys. Res.* **119**(7), 4204–4227.

Ekelund, R., Eriksson, P. and Pfreundschuh, S.: 2020, Using passive and active observations at microwave and sub-millimetre wavelengths to constrain ice particle models, *Atmos. Meas. Tech.* **13**(2), 501–520.

Ellison, W.: 2007, Permittivity of pure water, at standard atmospheric pressure, over the frequency range 0–25 thz and the temperature range 0–100 c, *Journal of physical and chemical reference data* **36**(1), 1–18.

Eriksson, P., Buehler, S. A., Davis, C. P., Emde, C. and Lemke, O.: 2011, ARTS, the atmospheric radiative transfer simulator, version 2, *J. Quant. Spectrosc. Radiat. Transfer* **112**, 1551–1558.

Eriksson, P., Ekelund, R., Mendrok, J., Brath, M., Lemke, O. and Buehler, S. A.: 2018, A general database of hydrometeor single scattering properties at microwave and sub-millimetre wavelengths, *Earth Syst. Sci. Data* **10**(3), 1301–1326.

Eriksson, P., Rydberg, B., Mattioli, V., Thoss, A., Accadia, C., Klein, U. and Buehler, S. A.: 2020, Towards an operational ice cloud imager (ICI) retrieval product, *Atmos. Meas. Tech.* **13**(1), 53–71.

Evans, K. F. and Stephens, G. L.: 1995, Microwave radiative transfer through clouds composed of realistically shaped ice crystals. part ii: Remote sensing of ice clouds, *J. Atmos. Sci.* **52**, 2058–2072.

Liebe, H. J.: 1989, MPM – an atmospheric millimeter–wave propagation model, *Int. J. Inf. Millim. Waves* **10**(6), 631–650.

Pfreundschuh, S., Eriksson, P., Duncan, D., Rydberg, B., Håkansson, N. and Thoss, A.: 2018, A neural network approach to estimating a posteriori distributions of bayesian retrieval problems, *Atmos. Meas. Tech.* **11**(8), 4627–4643.

Prigent, C., Aires, F., Wang, D., Fox, S. and Harlow, C.: 2017, Sea-surface emissivity parametrization from microwaves to millimetre waves, *Q. J. R. Meteorol. Soc.* **143**(702), 596–605.

Rosenkranz, P. W.: 1993, Absorption of microwaves by atmospheric gases, *in* M. A. Janssen (ed.), *Atmospheric remote sensing by microwave radiometry*, John Wiley & Sons, Inc., pp. 37–90.

Rydberg, B., Eriksson, P., Buehler, S. A. and Murtagh, D. P.: 2009, Non-gaussian bayesian retrieval of tropical upper tropospheric cloud ice and water vapour from Odin-SMR measurements, *Atmos. Meas. Tech.* **2**(2), 621–637.

Saunders, R., Hocking, J., Turner, E., Rayer, P., Rundle, D., Brunel, P., Vidot, J., Roquet, P., Matricardi, M., Geer, A. et al.: 2018, An update on the RTTOV fast radiative transfer model (currently at version 12), *Geosci. Model Dev.* **11**(7).

Sreerekha, T., Doherty, A., English, S. and Rayer, P.: 2008, The potential of Microwave Sounder 229 GHz channel, final report, *Technical Report EUMETSAT Contract EUM/CO/07/4600000409/CJA*, Met Office.

Stephens, G. L., Vane, D. G., Boain, R. J., Mace, G. G., Sassen, K., Wang, Z., Illingworth, A. J., O'connor, E. J., Rossow, W. B., Durden, S. L., Miller, S. D., Austin, R. T., Benedetti, A., Mitrescu, C. and the CloudSat Science Team: 2002, The CloudSat Mission and the A-Train: A New Dimension of Space-Based Observations of Clouds and Precipitation, *Bull. Amer. Met. Soc.* **83**(12), 1771–1790.

Turner, E., Rayer, P. and Saunders, R.: 2019, AMSUTRAN: A microwave transmittance code for satellite remote sensing, *J. Quant. Spectrosc. Radiat. Transfer* **227**, 117–129.